Design of a pneumatic Dual-Drive Planetary actuator to improve the velocity of MR guided manipulators

M. (Michael) ten Den

MSc Report

Committee:
Prof.dr.ir. S. Stramigioli
V. Groenhuis, MSc
Dr. F.J. Siepel
Dr.ir. F.F.J. Simonis
Ir. P. Krechting

September 2017

043RAM2017
Robotics and Mechatronics
EE-Math-CS
University of Twente
P.O. Box 217
7500 AE Enschede
The Netherlands

UNIVERSITY OF TWENTE.

MIRA
BIOMEDICAL TECHNOLOGY
AND TECHNICAL MEDICINE

CTIT

Abstract

MRI is one of the imaging techniques to diagnosis prostate cancer (PCa) and guide an intervention. Prostate biopsies performed with the MRI are time-consuming and difficult to perform accurately because of the space constraint caused by the closed bore of the MR scanner. MR guided manipulators address this problem by providing accessibility and position accuracy. However, the design of manipulators are limited in material and actuation type due to the magnetic field of the MRI. State-of-the-art MR safe pneumatic actuators show high potential results, but lack of bandwidth (i.e. low output velocity and/or accuracy), because they are connected to 6 m long hoses between the control room and the MR scanner. A new design is of the actuators is required: one that can increase the velocity of the actuators, while maintaining the required biopsy accuracy.

This thesis presents a MR safe pneumatic Dual-Drive Planetary actuator (DDPa) which enables fast and accurate stepping motion in a MR environment. The actuator merges the motion of two rotary pneumatic stepper motors using a planetary gear and transforms the rotary motion with a rack-pinion mechanism to deliver both a fine and coarse linear output velocity. A novel ring actuator (RA) with a circular rack is developed to actuate the ring gear of the planetary gear. The fine and coarse motion of the actuator delivers an output displacement of respectively 0.49 mm/step and 3.9 mm/step with a precision of 0.06 mm/step and 0.2 mm/step. A stepping frequency up to 18 Hz is achieved with 6 m long hoses, resulting in velocities up to 70 mm/sec, which is about a factor 3 increase compared with previous designs. Apart from this, the actuator can lift a force up to 90 N at a pressure of 0.3 MPa.

The proposed Dual-Drive Planetary actuator brings MR guided prostate biopsies a step closer towards a less time consuming biopsy procedure by increasing the velocity for MR Safe pneumatic actuators, while maintaining a high accuracy.

Acknowledgement

So this is it, my final thesis, lying now in front of you. I had a hard time writing this piece of art. Fortunately, I got a lot of pleasure from designing and building my actuator. It was great to work on this topic, and would like to thank the RAM group and DEMCON for this.

At RAM, I would like to thank my daily supervisors, Vincent and Françoise, for guiding me with their kindness through this great adventure of graduating. We had great and inspiring conversations. I would also like to thank Gerben and Eamon, for their support in the mechanical design and also Gerben for giving the possibility to 3D print my design.

At DEMCON, I would like to thank Benno for initiating this opportunity. I would also like to thank Peter and Maarten for their supervision and support on the other side of the street.

Have fun with reading this report,

Michael ten Den
info@michaeltenden.nl

Contents

1 Introduction

Prostate cancer (PCa) is the second most common cancer among men. Fifteen percent of men diagnosed with cancer, suffers from this type. Currently, it is the fifth leading cause of death from cancer worldwide, with a mortality rate of 6.6% [1].

The conventional method for PCa screening consists of a prostate-specific antigen (PSA) test combined with a transrectal ultrasound (TRUS) biopsy - ultrasound images obtained by sound waves. This method is beneficial to PET and CT scans, since TRUS is a non-radiant imaging technique. During a prostate biopsy, several pieces of the tissue or cells from the potentional PCa area on the prostate gland are extracted. The samples are examined under a microscope to determine if the sample contains cancer- or other abnormal cells.

One of the disadvantages of PSA testing is the difficulty in detecting early stage PCa. A Magnetic Resonance Imaging (MRI) scan is more advanced and better in distinguishing the risk of a PCa lesion. The MRI is benificial over TRUS, since it is more accurate in localizing the PCa lesion. TRUS guided biopsies require numerous samples (14 - 18) to be acquired, whereas the MR method requires 2-3 samples [2].

Despite the advantages of MR guided biopsies, TRUS is still the standard detection method in most hospitals. The main reasons for this are the lower costs and the shorter operating times of the TRUS method. The MR guided method requires a qualified technician to operate the MR scanner. Furthermore, the physician needs to switch between the treatment room and the MR control room for several times to evaluate the position of the needle in the patient's body [3]. As result, a conventional TRUS guided biopsy is significantly faster (15-20 minutes) then a MR guided biopsy (23-65 minutes).

In short, one TRUS device can treat more patients in a day and requires less employees. However, this method is less accurate compared to the MR method in detecting PCa.

Higher accuracy in a MR guided biopsy is required to decrease the biopsy time, because less samples need to be extracted and the number of evaluations steps performed by the physician are reduced. Robotics systems are developed to improve the biopsy accuracy, however it is a challenging task due to the MR environment. The magnetic field created by the MR scanner restricts the material use and actuation methods of the robotic system. The use of wrong materials results in a hazardous situation for both the patient and the physician. A MR compatible material can still distort the imaging of the scanner in case an incorrect actuation technique is used. The hazard and distortion can be prevented by only using materials and actuation techniques that are classified as *MR safe*.

A method of MR safe actuation techniques is the pneumatic actuation. It is fast and hygienic. Compressibility of air and friction in the system makes continuously driven pneumatic actuators difficult to control and limits its precision. A discrete pneumatic actuator - the pneumatic stepper motor - is suitable for accurate position control. Several pneumatic stepper motors, like the PneuStep [4] and the T-63 [5], are created for MRI purposes. Exceptional results are achieved with these stepper motors in lab setups and both studies are presenting a robot that operates in a MR environment.

1.1 Problem statement

A suitable pneumatic actuator for the MR guided robot is fast and accurate. The current state of the art in pneumatic actuators for MR guided biopsy are not fast or accurate enough to lead to significant time reduction. The PneuStep has a maximum step frequency of 10 Hz, and a experimental 20 Hz, and the T-63 a maximum of 11 Hz, when actuated with six meter long hoses. The maximum stepping frequency of these actuators is significantly influenced by the length of the hoses between the actuators and the pneumatic controller because of the limitations given by the dynamics and compressibility of air. These limitations directly result in the research question of this thesis:

Research question 1. *Can a MR Safe pneumatic actuator be used to significant reduce the time of a MR guided biopsy?*

The pneumatic controller is not MR Safe, hence it needs to be placed outside the MR room. Therefore, a pneumatic actuator placed in the MR scanner requires six meter long hoses to be actuated. The long hoses limits the actuator to a maximum stepping frequency to 11 Hz. Higher output velocity can be achieved by increasing the step size of the pneumatic actuator. However, it negatively affects the accuracy of the actuator. Hence the second research question is:

Research question 2. *How can the velocity of pneumatic actuators be improved, while maintaining the required accuracy?*

1.2 Thesis outline

This thesis starts with relevant background in Chapter 2 about pneumatics systems in MRI and mechanisms to improve the velocity. Chapter 3 provides the requirements for the actuator and presents the proposed design. Furthermore a description of the experiments that will be done are given. Chapter 4 presents the results of the experiments and provides the discussion. Answering the research questions and concluding this researsch is given in Chapter 5.

2 Background

In order to thoroughly understand the design challenges, background information about MRI and the current state of research is provided.

To give answer to the first research question, background information about the MRI and how it affects the usage of material is required (Section 2.1). Next, the state of the art of current actuation techniques in MRI is evaluated and a set of existing MR-Safe pneumatic actuators are presented (Section 2.2). Existing robotic manipulators for MR guided prostate biopsy together with the biopsy methods and the workflow of a biopsy are examined (Section 2.2.3).

The origin of the second research question is found in the limited stepping frequency caused by the long pneumatic hoses. The aim of this research is to increase the velocity of pneumatic actuators, thus the movement speed of a MR guided pneumatic robot, while maintaining the stepping accuracy of the actuator for precise movement during biopsy. A method to reduce the length of the hose, i.e. developing a MR Safe pneumatic controller, is outside the scope of this research.

A transmission will be considered, as using transmission ratios it can be possible to increase the output velocity. A few types of transmission are evaluated in Section 2.3.1. As result of the velocity change, the accuracy is altered too. To obtain proper accuracy, while increasing the velocity, two options are discussed: 1) A shifting mechanism is implemented to shift between different ratios (Section 2.3.2); 2) Multiple actuators are combined to deliver the high-speed and the accurate positioning (Section 2.3.3).

2.1 Magnetic resonance imaging (MRI)

Magnetic resonance imaging, better known as MRI, uses a strong static magnetic field to align the spin of hydrogen nuclei (protons) inside a body. Adding additional energy to the magnetic field by exciting an radio wave frequency (RF) onto the body, the hydrogen nuclei starts to resonate. The frequency to resonate depends on the type of element (e.g. hydrogen) and the strength of the magnetic field. Electric coils are used to create a variable magnetic field over the total body in X,Y,Z direction. By exciting different RF signals will result in resonating different slices of the body. A cutaway of a closed-bore MR scanner is illustrated in Figure 2.1.

Switching the RF source off will cause the hydrogen nuclei to return to their rest state. This transition causes emitting a RF signal and this is captured by receiver coils radio. The intensity of the received signal is mapped to the well known gray scale images (slices). Since a human body consist mostly out of water (H_2O), which contains hydrogen nuclei (protons), the MRI is good in detecting abnormalities in body tissues [6].

Image guidance biopsies can be performed with various techniques, like computed tomography (CT), MRI, PET and ultrasound. CT- and PET scan uses radioactive radiation to create an image of the patient, which has a negative effect on the health of the patient. MRI and TRUS are using respectively magnetic and ultrasound waves for imaging, hence the patient is not exposed to ionized radiation. MRI capabilities have advanced significantly in clinical practice by adapting a higher static magnetic fields, such as higher signal-to-noise (SNR) and contrast-to-noise (CNR) ratio, but also sensitivity of soft tissue, decreased imaging times and increased spatial resolution [7, 8].

This relatively new detection method has shown a significant raise in the detection rate from 22% (for the TRUS method) up to 47-64% [9]. The study of Schouten et al. that in a MR guided biopsy the location of the lesion can be determined more accurately [10]. Therefore, the number of biopsies per lesion can be reduced from 10-14 needles (for the TRUS guided method) to 2-3 needles [2].

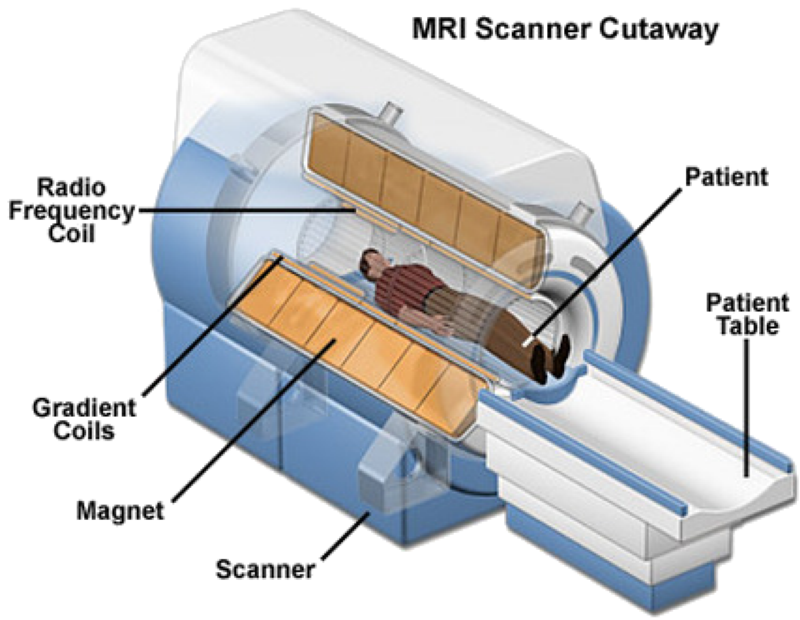

Figure 2.1: Cutaway of closed-bore MRI scanner, obtained from [11]

2.1.1 Safety definitions for in a MR environment

Due to strong gradients towards the bore, produced by the high static magnetic field, any ferromagnetic and high paramagnetic material will be attracted with strong forces towards the bore. Furthermore, the emitted RF signal by the MRI scanner can cause eddy currents and strong heating in conductive material. Therefore, medical devices should be made of non-magnetic, non-metallic and non-conducting materials. Metal, like aluminum, not a suitable construction material for medical devices in MR environment.

A medical device should be safe to use in a MR environment and not interfere with the fMRI image. It must not harm or endanger the radiologist or patient. The American Society for Testing and Materials (ASTM) created the technical standard F2503 that describes the safety definitions for a MR environment. In 2005 the ASTM released an update of the definitions, due to unclear and misuse of the historical terms *MR Safe* and *MR Compatible* [12]. *MR compatible* is removed from the list and a new term *MR Conditional* is introduced. The new definitions of the terms, and referred to in this report, are:

> MR Safe: "*an item that poses no known hazards in all MR environments*" [13, 3.1.10].
>
> MR Conditional: "*an item that has been demonstrated to pose no known hazards in a specified MR environment with specified conditions of use.*"[13, 3.1.9].
>
> MR Unsafe: "*an item that is known to pose hazards in all MR environments.*"[13, 3.1.11].

Materials which are inherently MR Safe are plastics, glass and rubber.

2.2 Actuation in a MR environment

Actuators suited for use in MR environment cannot endanger the patient or radiologist. Furthermore, they may not affect the quality of the image quality. Therefore, conventional electromagnetic actuators cannot be used, since its driving principle is based on magnetism. Electrically controlled piezo- [14, 15, 16] and ultrasonic actuators [17] exist, but are labeled MR Conditional. Fischer et al. shows that these categories of actuators deteriorate the image quality [18]. Not to mention, the actuators are a potential danger when applied in MR scanners with higher field strengths.

This section goes into detail about MR Safe actuation and state of the art MR guided robots. Since pneumatic actuation will be used in this thesis, this section will first elaborate the possible actuation principles (Section 2.2) and present the performance of the state of the art pneumatic stepper motors (Section 2.2.2). Next, developed MR guided robots for prostate biopsy are presented and, together with the biopsy workflow, investigated for improvement (Section 2.2.3). Minimizing the time to target the robot to the location of the lesion reduces the biopsy time significantly, however this is limited by the length of the hoses. Insight about the effect of the hoses on the actuator speed is given in Section 2.2.4.

2.2.1 MR Safe actuation

Currently, MR safe actuation is limited to two techniques: 1) Mechanical; and 2) Fluid. The fluid actuation can be divided in: 1) Pneumatic (gas as medium); and 2) Hydraulic (liquid as medium). A brief description of each method is provided in this section after elaborating the actuators' controller in MR environment.

The controller for the three actuation types is not MR safe and is therefore placed in the control room of the MRI, which is located next to the MR room. Placing the controller in a shielded box, to reduce image deteriation, inside the MR room is possible, however this inherently is not MR safe, thus considered as unsuitable. In a hospital, the distance of transit between the MR scanner and control room can be assumed to be six meter, which is consistent with other reports [19].

Bowden cable A bowden cable is a mechanical approach for MR safe actuation in a MR environment. It consist of a outer tube and an inner cable and is used as pulling mechanism. Chapuis et al. presents a cable transmission with a 9 mKevlar rope, where they achieve a bandwidth of 30 Hz [20]. The inertia of the ropes are low, hence a higher bandwidth can be achieved compared with a fluid transmission. The stiffness of the cable transmission is of the same order as that of the hydrostatic transmission. The presented setup cannot be applied in a MR environment. The system needs to be converted to a setup with a bowden cable to guide the Kevlar rope to the actuator in the MR room. The movement of the Kevlar rope in the bowden cable will results in higher friction, which will limit the bandwidth of the system. This is not discussed in the study, hence the effect of the friction on the bandwidth is unknown.

Fluid power Another solution for the actuation is the use of pressurized fluid, since this actuation principle is inherently MR safe. In case of a hydraulic fluid actuator, the fluid is oil, or less common water, while in pneumatic the fluid is air.

A study done by Ganesh et al. uses a hydraulic fluid system for MR environment [21]. An *master* actuator is connected by two hydraulic pipes to a passive *slave* mechanism. A bandwidth of 20 Hz is achieved with a hose-length of 6 m. The study shows that the bandwidth is primary limited on the hose length and minor by the hose diameter.

A comparison study between pneumatic and hydraulic system is performed by Yu et al. [22]. Hydraulics scores in smoother movement and robustness against force disturbances, whereas pneumatic results in better and faster force control performance.

Pneumatic actuation is preferred, since it works on lower pressure and has no hygienic problems for the patient when leaking occurs.

2.2.2 Pneumatic stepper motors

Continuous pneumatic motors (like a vane motor) rotate constantly and change their angular velocity by changing the pressure on the motor. These motors can be driven at much higher speed, even with a small bandwidth, however feedback is required to obtain the position. Therefore a MR safe position sensor is required. Furthermore, position control of these type of actuators is a challenging task due to the time-delay introduced by the long hoses.

A pneumatic stepper motor can be easily controlled on the position, independent of the possible bandwidth. The stepper motors are more robust on position, when external forces are applied. In contrast, its velocity is depending on the bandwidth. A decrease in bandwidth results in a slower actuator, hence a longer settling-time.

Stoianovici et al. developed the pneumatic actuator *PneuStep*, it is created from fully MR compatible materials and implemented in a prostate biopsy robot [4]. The motor has a 3.3° rotational with a linear step size of 0.055 mm linear step size. The actuators uses three pistons that created together 6 steps with a maximum speed of 60 steps/ sec with a custom-made distributor and 120 steps/ sec with an electroniccaly controlled distributor. The author thinks the increase of factor two is a result of a faster opening time of the valves. The speed declines rapidly when the output torque is increased [4]. The actuator is an interesting, but complex design which require many components for construction (26 components from 11 different materials). Groenhuis and Stramigioli presented a set of rotational and linear stepper motor with high torque / force output for MR compatible actuators [5]. The author has focused on creating a design which is printable with an off-the-shelf 3D printer and uses only six different components. Drawback of the system is the accuracy of the systems, due to large step sizes, and low operating frequency (11 Hz with 6 m long hoses).

2.2.3 Pneumatic robotic manipulators for MR guided prostate biopsy

In a prostate biopsy, prostate gland tissue is taken out with a biopsy needle or during surgery. The tissue is checked to see if there are cancer or other abnormal cells in the prostate gland. A prostate biopsy may be done in several different ways:

- Transrectal method: The rectum is used to access the prostate gland
- Perineal method: The prostate is accessed through the skin between the scrotum and the rectum
- Transurethral method: The prostate is reached by the penis, through the urethra, up to the gland.

The MIRIAM manipulator uses the perineal method to perform biopsies [15]. The patient is placed in semi-lithotomy position to access the perineal skin. This position reduces the obstructions to access the prostate (see Figure 2.2, the legs of the patient are left out).

Biopsy time Zangos et al. presents a MR-compatible robot guidance with a median intervention time of 39 minutes (range 23 to 65 minutes) [23]. In this study the biopsy is performed with a percutaneous insertion with a median needle travel distance from the insertion point to the target point of 13.2 cm(range 9.9 to 13.8 cm). Zamecnik et al. presents a real-time needle tracker to improve the biopsy time to a range of 14 - 48 minutes with a median of 32 minutes using the transrectal approach [3]. The median time for guidance per target, which is the movement of the needle between two lesions, was 1.5 minutes (range 0.7-5 minutes).

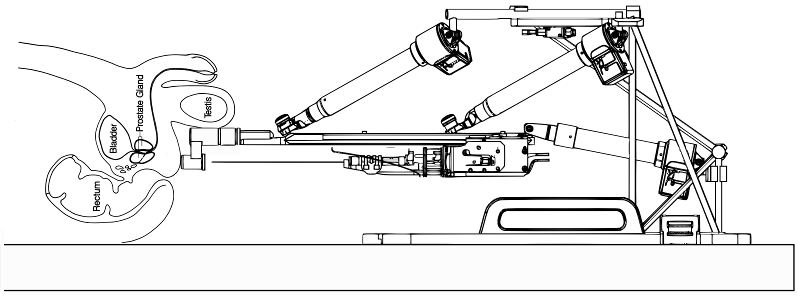

Figure 2.2: Illustration of MIRIAM in the prostate biopsy setup

Another MR compatible manipulator is developed by Soteria Medical BV, using the transrectal path, and Bomers et al. examined its feasibility [24]. This manipulator uses cylindrical pneumatic stepper motors to positioning and steer the needle. The median procedure time was around 37 minutes (range 23 - 61 minutes) and the median guidance per target was 5:48 min (1:25 - 18:35 minutes). One major factor of improvement here is the ability to track the needle real-time, so steering of the needle could be done immediately by the radiologist. This removes the step of the radiologist walking from the patient to the control room and back to adjust the needle.

A 'MRI Stealth' robot is developed by Stoianovici et al. and is constructed with several pneumatic stepper motor called Pneustep [4]. This manipulator achieves an average position error within the 0.315 mm (SD: 0.143 mm). No time for taking biopsy is not given. To not endanger the patient during the intervention, Stoianovici et al. writes that the maximum speed of the needle should not exceed the 20 mm/ sec when inserted in the patient.

The required accuracy for a MR guided robot depends on the size of the tumor. According to Stamey et al. tumor in the prostate with a volume of less then 0.5 cm^3 is often an insignificant prostate cancer (Ins-PCa) [25]. This means that the tumor will not result into cancer during the life span of the patient. To determine the radius of the tumor, a spherical model is used for approximate. The radius of the sphere can be derived with the spherical volume and is given by

$$V = \frac{4}{3}\pi r^3 \tag{2.1}$$

$$r = \sqrt[3]{\frac{3V}{4\pi}} \tag{2.2}$$

A volume of 0.5 cm^3 gives a radius of approximately 5 mm. Zamecnik et al. reports that the median of maximum diameter of the regions suspicious for cancer is smaller, i.e. 8 mm (range 4 to 13 mm [3]. In a personal email interview with doctor J. Fütterer, Interventional-Radiologist at Radboud university medical center, an accuracy of less then 2 mm is preferred as they perform biopsy on lesions with a radius of 2.5 mm.

Fütterer writes that the primarily improvement to reduce the biopsy time is to reduce the time for guidance per target. Fast movement reduces the time of positioning the robot in target direction, whereas an accurate robot lessen the number of walks of the radiologist between the control room and the patient. Full path planning with a fast and accurate robot is considered as the optimal combination for biopsy time reduction.

Internal documents from [26][1] show that the procedure of taking one biopt with a full planning robot takes around 8 minutes. The steps with the estimated time for acquiring one biopt is displayed in Table 2.1. Acquiring 4 samples results in 32:20 min.

[1] Source derived from the intranet (not publicly available) of DEMCON.

Workflow	Action	Duration (h:mm:ss)	Cumulative (h:mm:ss)
08	Table moves into bore	0:00:20	0:00:20
	Localizer scan	0:00:20	0:00:40
	Pre-op scan from prostate and needle guide	0:00:30	0:01:10
	Sum workflow	**0:01:10**	-
09	Clinician selects target point	0:00:30	0:01:40
	Robot places needle guide on entry point	0:00:30	0:02:10
	Sum workflow	**0:01:00**	-
10	Calculate path	0:00:30	0:02:40
	Insert needle 30 mm, step 1-5	0:00:10 (5×)	0:03:30
	Make MR image (orthogonal slides), step 1-5	0:00:10 (5×)	0:04:20
	Sum workflow	**0:02:10**	-
11	Approve target location	0:00:30	0:04:50
	Fire needle	0:00:30	0:05:20
	Retract needle	0:00:30	0:05:50
	Sum workflow	**0:01:30**	-
12	Table moves out of bore	0:00:20	0:06:10
	Retract robot from ground plate	0:00:10	0:06:20
	Retract cannula	0:00:05	0:06:25
	Sum workflow	**0:00:35**	-
13	Release biopsy in sterile container	0:00:10	0:06:35
	Retreat stylet and needle robot back in ground plate	0:00:30	0:07:05
	Robot moves in nominal position	0:01:00	0:08:05
	Sum workflow	**0:01:40**	-
	Total time	-	**0:08:05**

Table 2.1: The intended workflow with action and time for a transperineal prostate biopsy using the MIRIAM system. During this biopsy the patient is in semi-lithotomy position.

2.2.4 Effect of pneumatics in MR environment

As mentioned in Section 2.2.1, the power source, electronics and pneumatic valves to actuate the robot, cannot be placed in the MR room.

The hose between the pneumatic valves and the actuators is 6 m long. High bandwidth is difficult with this relative large distance, and is limited by the compressibility of air and the highly turbulent flow through the tubes (which results in higher tube friction coefficient). Furthermore, at the beginning of the inflation process, a dead time of $\Delta t = L_{tube}/C$, caused by the maximum speed of sound in air with $C = 343\,\mathrm{m/sec}$ for $T = 293\,\mathrm{K}$. For a tube with a length of $L_{tube} = 6\,\mathrm{m}$ the dead time is $\Delta t = 6/343 \approx 1.7 \times 10^{-3}$ sec.

The lowest natural frequency of the air column in the tube dominates the output response of the pressure at the end of the tube at these long distances. This frequency can be estimated with:

$$f_{tube} = C/(4 \cdot L_{tube}) \tag{2.3}$$

where f_{tube} is the lowest natural frequency of the tube in Hertz and C is the speed of sound [27].

The lowest natural frequency for a tube of 6 m is $f_{tube} = 343/(4 \cdot 6) \approx 14.3\,\mathrm{Hz}$. Combine this frequency with the dead time results in a final response frequency of $\approx 11.4\,\mathrm{Hz}$.

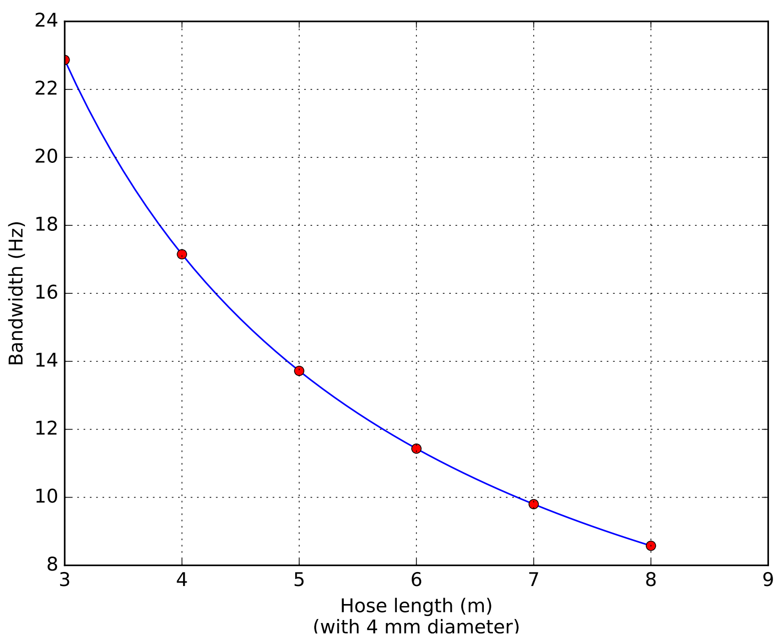

Figure 2.3: Frequency of pressure response for different tube lengths.

2.3 Transmission mechanisms to increase the velocity

The section goes deeper in the current approaches to increase the output velocity of an actuator, while maintaining the accuracy.

2.3.1 Types of transmission

The stepping frequency is fixed, hence the transmission ratio of the actuator needs to be altered to increase the output velocity of the actuator. If the output of the actuator is rotary, a gearbox can attached to the output shaft of the actuator to increase the output velocity. The function of a gearbox is to transmit power from the input to the output shaft, while the velocity of the shafts can differ. A list of common transmission mechanism in automobile industries and robotic actuators are:

- Continuous Variable Transmission (CVT)
- Parallel axis gear transmissions
- Planetary gear transmission [2].

Each mechanism can be used stand-alone, but there are also examples where two of the listed mechanisms are combined. For example, planetary gears are often found in CVT's to enable a reverse gear without changing the rotating direction of the motor.

Continuous Variable Transmission A CVT has, unlike conventional transmission, infinite gear ratios within a limited range. The CVT can change its ratio without interruption, hence the name *continuous*. This feature enables the power source connected to the CVT to rotate at an optimal speed, which often is when the power source is rotating most efficient or delivering the highest power or torque.

CVT's exist in multiple domains, where the most common are: (1) Mechanical; (2) hydrostatic; and (3) electric [28, 29]. In our interest, the mechanical category can be divided into: (1) toroidal; (2) ball toroidal; (3) belt; and (4) chain [30]. The most common found in automotive applications is the belt and chain type, whereas the ball toroidal is found in bicycles for electric bikes (NuVinci).

According to Spanoudakis and Tsourveloudis the efficiency of a belt driven CVT lies around 89% [30]. Efficiency of toroidal CVTs lies around the 91%, but a fluid is required inside the transmission to achieve this efficiency.

Advantage of a CVT is the continuous transition with infinite transmission ratios. As result from this feature, a CVT is a complex system which give high manufacturing costs.

Parallel axis transmission Parallel axis transmissions consist of two or more gears meshing with each other with parallel rotation axes (see left image of Figure 2.4). The ratio for the transmission is determined by the first and last gear. Intermediate gears are used to bridging the space between the input and output shaft. A compound of gear trains [3] can be used to create a large transmission ratio, without necessary increase the diameters of the input and output diameter. Parallel gears have a relative low production cost, since the manufacturing process is uncomplicated. Disadvantages of this transmission are high stress on the gear teeth and the gears slip.

Planetary transmission A planetary transmission is a gear system consisting of four parts: (1) sun gear; (2) multiple planet gears; (3) carrier; and (4) ring gear. One or multiple *planet* gears

[2] In literature two definitions of the term *planetary gear* are found: 1) synonym for Epicycle gear; 2) specific an epicycle gear with fixed ring gear. The first definition is most common in papers and there for used in this report.

[3] Gear train: A set of multiple meshing gears.

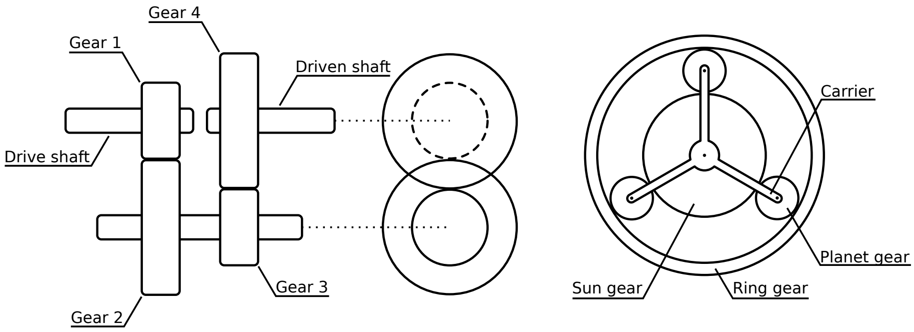

Figure 2.4: A parallel and planetary gear

are revolving around the in the center located *sun* gear, while rotating around their own axes at the same time. These gears act as idle gears and cannot be used as input or output element. A *carrier* is connected to the planet gears to hold these gears in position. A *ring*, or annular, gear is located outside the orbit of the planet gears and meshes with the planet gears. The sun gear, ring gear and carrier are all revolving around the same central axis and can be used as input or output element of the gear system. An illustration of a planetary transmission is presented in the right image of Figure 2.4.

In hybrid power trains the planetary gear acts as a differential and is used to add the power of the electric motor to the power output. These type of power transmissions are called power-split CVT's, where the planetary gear is responsible for the power splitting [31]. In the hybrid situation the planetary gear has two degrees of freedom (DOF). To obtain a fixed input-output transmission ratio, one element is constraining to the fixed world to obtain an one DOF system.

Advantages of planetary gear trains is the possibility to create small volume and lightweight power transmissions. Furthermore a higher level of stiffness is achieved and gear slip is minimized, because the power is shared over a large amount of meshing tooth surface area [32]. From a manufacturing point of view, the planetary gear has high production cost caused by the complex design and the number of required gears.

2.3.2 Single actuator switching mechanism

In previous section three types of transmission are discussed. The CVT has the advantages over the other two to create infinite transmission ratios between two outer ratios. However this feature adds a lot of complexity to the system. Furthermore, the manufacturing is hard because of the limited use of materials. Therefore, constructing a MR Safe CVT is considered as unreachable within this research.

To switch in transmission ratio, three gear switching which are common in automotive are reviewed. In automotive, the shifting gears are used to switch the transmission ratio between the engine and output shaft of the car. A low shift is required for slow, but powerful propulsion, where a higher gear is used to reach higher velocity while keeping the engine running in its effective speed range. The parallel axis transmission is used to illustrate the working of each switching mechanism. However, a sliding switching mechanism is also applicable on a planetary gear. For example, Wu and Chang presents a *sliding shaft* mechanism to change the gear ratio of a planetary gear inside a rear wheel hub of a bicycle [33].

A typical parallel axis transmission gearbox consist of a input shaft, a counter shaft and a output shaft. Input shaft is connected to the counter shaft with a fixed gear ratio. The counter shaft consist of multiple gears which are designed to mesh with the gears on the output shaft.

One of the simplest transmission in automotive is the *sliding mesh transmission* where the gears are fixed on the output shaft. The output shafts is moved, parallel to the counter

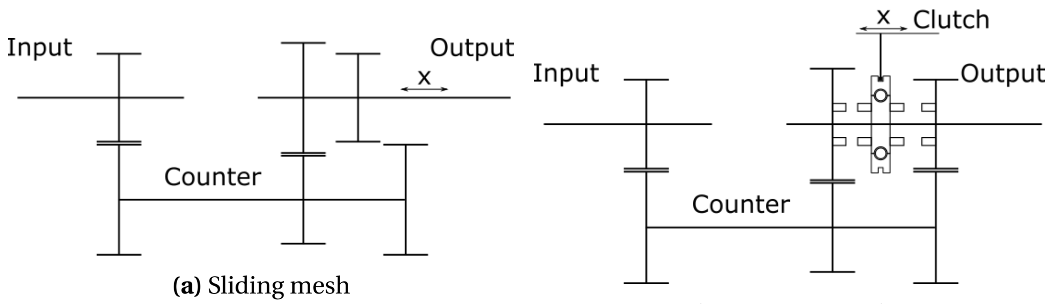

(a) Sliding mesh

(b) Constant mesh

Figure 2.5: Illustration of the sliding and constant mesh concepts

shaft, to shift gears (2.5a). A more advanced transmission in automotive is the *constant mesh transmission*, where the gears on the output shaft are free to rotate and always in mesh with the gears on the counter shaft (2.5b) A clutch[4] is used to engage or disengage with different gears to the output shaft. A fork shifter is used to shifts the clutch to the preferable gear. This transmission is known for its fast and precise shifting.

The disadvantages of both transmission is shifting between gears, while the shafts don't have the same speed results in grinding gears. This damages the dog ears of the clutch and gear. Therefore, most modern consumer applications are fitted with a *synchronized mesh transmission* to deliver a more smooth and reliable operation. A external cone is placed between the gear and the clutch to synchronize the speed of the clutch and gear before interlocking the two elements. The large dog ears are replaced by using splined sleeves on the clutch and the synchronizer.

All three switching mechanisms have the problem that the output shaft needs to be disengaged from the counter shaft, before shifting gear is possible. This results in a non-constraint output shaft while shifting gears, This means that the output rod of the actuator can be moved when shifting, hence the position of the output shaft with respect to the stepper motor becomes unknown. A non-back drivable mechanism, like a worm gear, or shaft locking mechanism can be used to prevent the output shaft from rotating.

2.3.3 Dual actuator driven systems

Constructing a pneumatic stepper actuator with large step size results in a high velocity, but lacks in accuracy. Using an actuator with smaller teeth results in smaller steps, hence higher accuracy is possible. Like the two sides of a coin, each actuator has its advantages, but at the same time they have a shortcoming. In case high speed and high precision are demanded at the same time, integrating both actuators in one system will overcome these shortcomings. This kind of system is referred to as a *dual stage system*. A distinguish can be made between *series* and *parallel* compounded system.

In the paper of Seki et al. a series coupled dual-stage actuator setup is presented [34]. A pneumatic actuator and a voice coil motor (VCM) are series coupled to expand the bandwidth of the system. The VCM has a fast response and can create fine movement, however the maximum reachable displacement is small. The pneumatic actuator is used to create the course movement of the systems, but has a low response bandwidth to slow servo response and resonant vibrations caused by pneumatic compressibility this actuator. By linking two actuators in series classical PID control on both actuators creates a resonant frequency due to the interference between both actuators. Control according the PQ method is proposed to suppress the resonant frequency and enables the option to do loop shaping for the overall system performance.

[4] Clutch: a disk with dog ears which interlock with the dog ears of the gears.

A novel actuator using parallel placed micro-macro actuator is presented by Morrell and Salisbury back in 1997 [35]. A *macro* actuator is used for high force output with low bandwidth force control, where a *micro* actuator enables high bandwidth force control with limited force output. Hoyul Lee et al. presents the system called *DuMP*[5]. This system uses two parallel placed actuators, connected to a pulley, to pull a object [36]. The actuators differ in specification to create the coarse and weak or the fine and strong pulling motion. Successor of DuMP is proposed in Lee and Choi and is called the *DuPG*[6]. The planetary gear is configured as a DISO (Double Input, Single Output) system, where one actuator is coupled to the ring gear and the other to the sun gear [37]. The actuator connected to the *Sun* gear produces the high speed of the system, where the other actuator produces the high torque required for the system. A worm gear is added to the output of both actuators to make the system non-back drivable.

The series coupled mechanism is focused on increasing the position resolution, whereas the parallel dual-stage actuator enables to achieve a higher force resolution In both type of dual-stage systems the actuators can be controlled simultaneously. Since the lack of a switching mechanism, the response time of these kind of systems are fast.

[5]DuMP stands for: Dual-motor system using movable pulley.
[6]DuPG stands for: Dual-motor system using a planetary gear.

3 Actuator Design

The previous chapter detailed the major challenges for fast and accurate pneumatic stepper motors in MR environment. This chapter proposes a design that overcomes these challenges.

Since this research is conducted in collaboration with DEMCON and the research group Robotics and Mechatronics (RAM) of the University of Twente, the design direction is biased.

Prior to this research, Groenhuis and Stramigioli developed a set of MR Safe pneumatic actuators at the RAM research group [5]. DEMCON developed a MR conditional robot designed for MR guided prostate biopsy called MIRIAM (Minimally Invasive Robotics In An MR environment) (see Figure 3.1). The MIRIAM system consist of a 5 DoF parallel system and a 4 DoF needle driver [15]. The position and orientation of the needle guide is achieved with the 5 DoF system, by five adjustable rods. Each rod is actuated by a piezoelectric motor (HR2 Nanomotion). The biopsy needle is inserted and rotated with the needle driver by using piezoelectric motors. In addition, a pneumatic actuator fires the biopsy needle to obtain a tissue sample.

This research intends to combine the work of both to become a step closer to a MR Safe prostate biopsy solution. Nonetheless, the proposed design is not limited to prostate biopsy, it is applicable in all MR guided applications.

The details of the proposed design are described in this chapter. First, the requirements of the design are determined in Section 3.1. Second, potential concepts are generated in Section 3.2. The best concept has been elaborated in detail in Section 3.3. Lastly, light is thrown upon the realization of the design (Section 3.4).

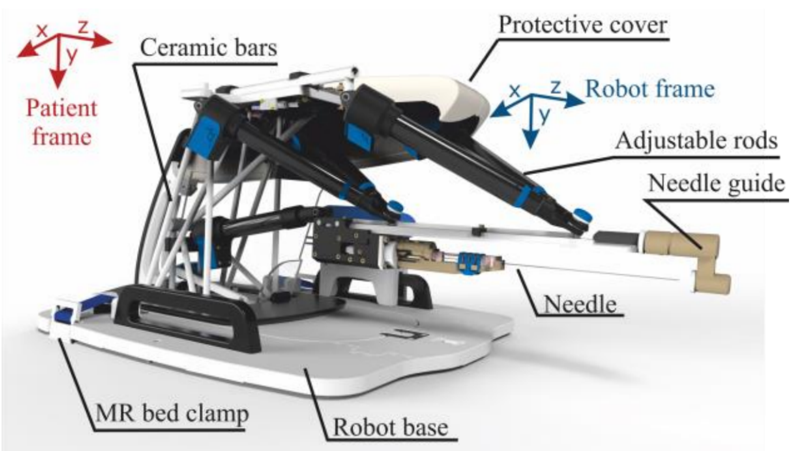

Figure 3.1: Render of MIRIAM, a MR conditional robot for needle steering with full path planning, obtained from [15]

3.1 Problem analysis

The aim of this thesis is to provide a Proof-of-Principle for replacing the actuators of the 5 DoF parallel system of MIRIAM with MR Safe actuators. In Figure 3.2 the actuators are highlighted and the distance between the joints on the end-effector rod, which holds the needle, are noted. The geometrical design of the parallel system is used to derive the requirements for the actuator.

To develop a safe actuator for MR environment, the actuator may only consist of MR safe material. Pneumatics with air as medium is used as actuation principle, chiefly because it works on relatively low pressure of $p = 6\,\text{bar}$, and cannot cause hygienic issues. The essentials of a MR guided robot is to have an accurate needle position system. For this reason pneumatic stepper motor are used.

To begin with, each required is described briefly. In addition, a label of priority is assigned to each requirement. An overview of all the requirements is presented in Table 3.1.

3.1.1 Requirements

R001 - Step size The required accuracy of the biopsy robot to sample the smallest lesion is 2 mm. The geometry of the biopsy robot is simplified by using a 2D model viewed from the side plane. This simplification and the distance between each joint on the needle guide is presented in Figure 3.2 of the needle For the worst case scenario it is assumed that back rods are connected perpendicular to the needle guide. The largest ratio is found in the situation that the needle of 200 mm is fully extended and the rotation point of the robot is found at the joint of the front rods. The corresponding ratio for this situation is $r_x = \frac{164\,\text{mm}+200\,\text{mm}}{250\,\text{mm}} \approx 1.46$, where 200 mm is the length of the needle and 164 mm and 250 mm are derived from Figure 3.2. The step size for the actuator is then $2\,\text{mm}/1.46 = 1.37\,\text{mm}$. The requirement for the step size is reduced to $s_{\text{acc}} = 0.5\,\text{mm}$ to enlarge the number of sample points in the lesions, so its center point can be localized more accurate.

R002- Velocity As mentioned in Section 2.2.4, a 6 m long hoses with a diameter of 3 mm limits the stepping frequency to a maximum of $f_c = 10\,\text{Hz}$. Reverse calculation of the minimum velocity of 40 mm/ sec results in a step size of $s_{\text{velo}} = 4\,\text{mm/step}$.

R003 - Static Force The rod of the actuator must be able to hold and move the tip of MIRIAM robot against gravity F_z, pretension F_{pre} and insertion force F_{ins}, in all possible configurations. The forces of $F_z = 20\,\text{N}$, $F_{\text{pre}} = 10\,\text{N}$ and $F_{\text{ins}} = 20\,\text{N}$ are combined in the worst case position. The rod must therefore be able to hold 195 N and move against a force of 88 N.

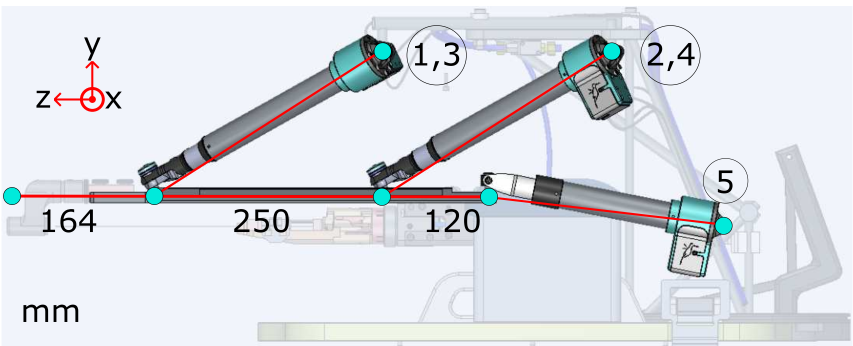

Figure 3.2: Side view of MIRIAM where the actuators (1 to 5) are highlighted and the distance between the actuator joints on the end-effector rod are presented.

The rods should be self-locking (i.e. not back-drivable) which means that it should maintain its position no matter what the pressure is. This specific detail is to prevent possible harmful situations for the patient.

R004 - Dynamic Force The dynamic force, e.g. the applied external force where the actuator does not stall, is derived with the same parameters as presented in requirement R003. The dynamic force of 88 N is calculated for each actuator.

R005 - Stiffness The maximum displacement of the rod when exposed to the maximum static force should be equal to the accuracy, which is 0.5 mm.

R006 - Range rod The single entry method of Van Gellekom et al. used in the biopsy procedure of MIRIAM to minimize the intervention [38]. This method, together with the design of MIRIAM, requires a rod elongation of 170 mm to cover the full prostate gland.

R007 - Dimensions The dimensions are based on the size of the current actuators, which volume is carefully studied in order for MIRIAM to be placed between the legs of the patient. The actuator fits in a tube with a total length of 275 mm. This is without the rod being extracted. The cross section of the tube is 85 mm.

3.1.2 Prioritization of the requirements

The important of each requirement is prioritized according the MoSCoW method with the label *must have*, *should have* or *could have*and listed in the last column of Table 3.1. The first label states any requirement that absolutely has to be achieved in order to consider the actuator successful. The second label is for requirements that needs to be in the overall deliverable, but are considered optional for the success of the actuator. The items with label must-have are weighted more throughout the design process.

The aim of this thesis is to deliver a Proof-of-Principle of a MR Safe pneumatic stepper actuator with increased velocity with accurate positioning. Therefore, the requirements *step size* and *velocity* are considered to be a must have.

Id	Requirement	Relation	Value	Unit	Priority
R001	Step size	<	0.5	mm	Must have
R002	Velocity	>	40	mm/ sec	Must have
R003	Static Force	>	195	N	Should have
R004	Dynamic Force	>	88	N	Should have
R005	Stiffness	<	0.5	mm	could have
R006	Range rod	>	169	mm	Could have
R007	Dimensions	<	$275 \times \oslash 85$	mm	Could have

Table 3.1: Requirements

3.2 Conceptual design

In the previous chapter the requirements and their priority are defined. The next step is to generate concepts with the focus on the primary priorities: step size and velocity.

Five concepts are generated in total, where two concepts are based on a single actuator use, whereas the other three use two actuators. The concepts are listed with their key features in Table 3.2 with a brief notation of their key features. Examination of the concepts is based on a Pugh chart.

3.2.1 Concept discussion

A comparison of the generated concepts is presented based on a Pugh chart in Table 3.3. The concepts are compared based on the requirements and, apart from this, on the self-locking property, the manufacturings process and the usability [1].

The single-drive concepts (concept 1 and 2) use sliding parts to change gear, as a consequence a design complexity for proper meshing is introduced, as well as friction between the sliding parts. In order to switch between gears, the external force should be minor, otherwise the friction between the sliding parts will be too much. Apart from this, if the switching mechanism is not designed properly, the output shaft can rotate freely when shifting gears and then the actual output position is unknown.

The three dual-driven concepts have a scattered pattern on their strongest and weakest points. The planetary gear concepts score on the step size, because an infinite number of steps can be produced for the coarse and fine movement. The spindle concept (concept 4) scores highest when dealing with the external forces. The novel actuator scores low on manufacturing, since it involves a new to be developed actuator. The spindle scores low on this item, because it involves a sliding part. The actuator with spindle is moved by the second actuator. Contrary, concept 3 scores high on this requirement, since it uses already developed actuators, which eases the manufacturing process.

3.2.2 Chosen concept

According to the scores in Table 3.3, the desired concepts are the dual-driven concepts. As mentioned in Section 3.1.2, the requirements *step size* and *velocity* are weighted more. This eliminates the spindle, because it cannot set infinite number of fine steps. In addition to the priorities, there is a tendency towards innovative concepts. For this reason, concept 5 is the proposed as actuator concept.

[1] Usability is scored on the ease of switching between accurate and high speed mode.

Key features	Concept render
• Sun gear as input, carrier as output • Use clutch to switch ring gear between fixed world ($\omega = 0\,\mathrm{rad/sec}$) and the sun gear ($\omega = \omega_{\mathrm{sun}}$) (ring gear is not visible on the render) • Combined with rack-pinion or spindle	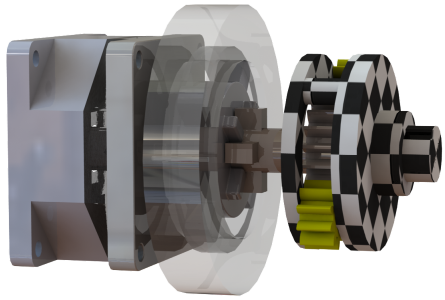
• Switches from sun to carrier by pressurizing piston • Grooved shaft meshes with splined gears • Combined with rack-pinion or spindle	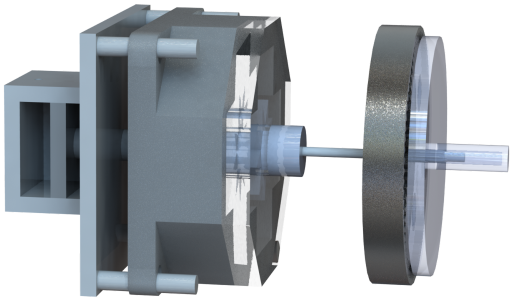
• Sun gear and carrier as output • Ring gear as pinion of the rack	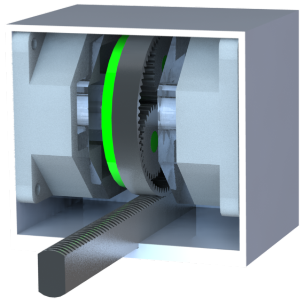
• First actuator spindle screw as output shaft • Spindle thread in the second actuator for fine movement • Second actuator equipped with spindle for coarse movement	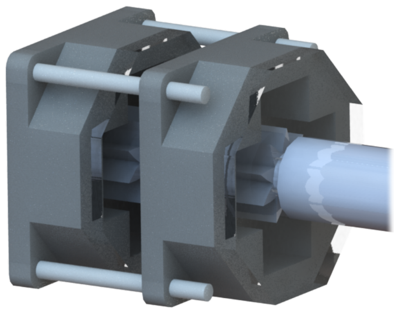
• Novel ring actuator for fine movement • Ring actuator for coarse movement. • Combined with rack-pinion or spindle	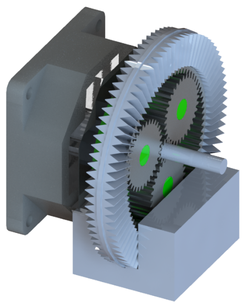

Table 3.2: Several concepts for the multi-variable velocity actuator. The first two concepts are single actuator driven with planetary gear as gearbox. The following two concepts are build with two rotary actuators. One with planetary gear as gearbox, the other only uses spindles. The latter concept consist of a rotary actuator and a novel ring actuator. A planetary gear is used as gearbox.

ID	Req.	Concept 1	Concept 2	Concept 3	Concept 4	Concept 5
		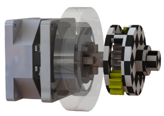	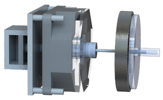	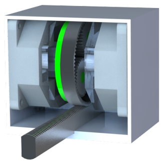	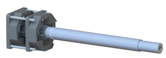	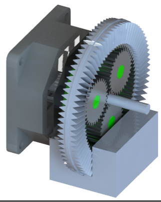
R001	Step size	+	+	++	+	++
R002	Velocity	-	-	++	-	++
R003	Static Force	-	-	-	++	-
R004	Dynamic Force	+	+	+	++	+
R005	Stiffness	+	+	+	+	+
R006	Range rod	+	+	+	+	+
R007	Dimensions	+	+	-	-	-
	Self locking	-	-	-	+	-
	Manufacturability	-	-	++	-	-
	Usability	-	-	+	+	+

Table 3.3: Comparison of the five concepts for the rod actuation. Rated with --, - , +, ++.

3.3 Detailed design

In this section, the concept of previous section is converted to a detailed design. A modular-based approach is applied to reduce design time per iteration by exposing mistakes in an early stage of the process.

First, a render of the proposed actuator design is presented in Figure 3.3, such that the reader is not puzzled with the design until the end of this chapter. The presented design consist of five modules, which are numbered in the figure and are as follows:

1. Housing: Acts as an interface by aligning all the modules and restricting their positions.
2. Rotary actuator: The first actuator, responsible for the coarse movement and is connected to the carrier.
3. Ring actuator: The second actuator, responsible for the fine movement and is connected to the ring gear.
4. Planetary gear: Acts as a differential by combining the rotary motion of the rotary- and ring actuator to the rack-pinion. The planetary gear consist of the following input/output elements: 1) Sun gear; 2) Ring gear; and 3) Carrier.
5. Rack-pinion: Converts the rotary output motion of the planetary gear to a linear motion.

Second, the design is created with a CAD program called *SolidWorks*. The *sun* gear and the *pinion* gear are first designed in their particular module and later on combined, such that parallel designing was possible. The *ring* gear and the *ring actuator* gear are also combined later on. The *housing* acts as the second interface, it aligns all the modules and fixes their positions.

The designs are equation-driven, such that a change in one module, updates all the other module. A script is written to calculate and optimize the planetary gear ratio. By performing

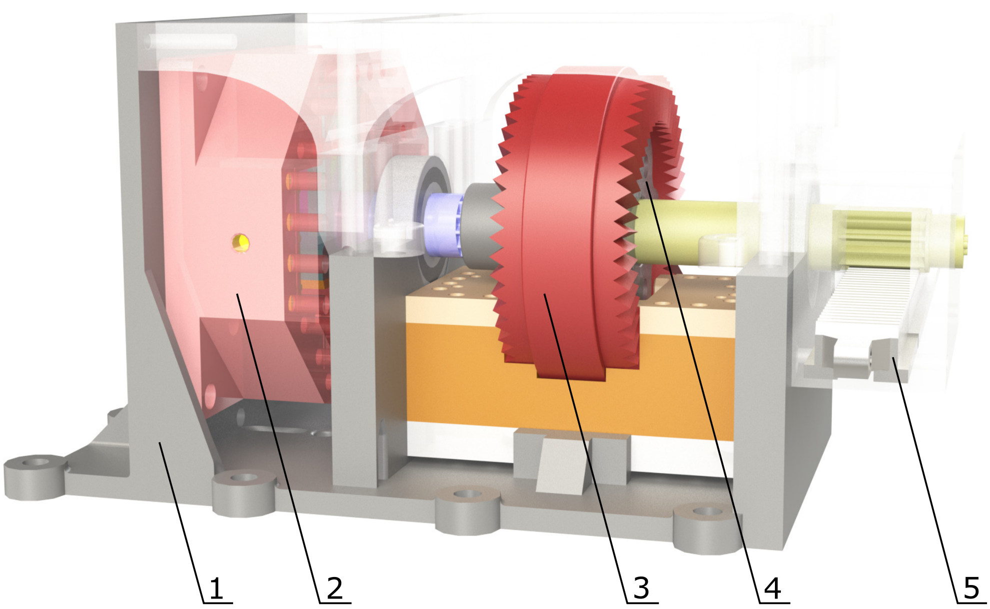

Figure 3.3: Render of the proposed design with the modules: 1) Housing; 2) Rotary (carrier) actuator; 3) Ring actuator; 4) Planetary gear; and 5) Rack-pinion

equation-driven design, *magic numbers*[2] are reduced to the absolute necessary, such that interface errors between the modules and their parts are avoided.

A detailed design of each module is described in the remainder of this chapter. To begin with, the design constraints, based on the requirements of Section 3.1.1, are described in Section 3.3.1. Second, the design of the planetary gear (Section 3.3.2) and the rack-pinion Section 3.3.3 are presented, which give the transmission ratios between the power of the actuators and the output rod. Next, the design of the ring- (Section 3.3.4) and rotary actuator (Section 3.3.5) are described. Lastly, the housing to assemble all modules together is presented in Section 3.3.6.

3.3.1 Design constraints

Constraints on the design are established based on the requirements presented in Section 3.1.1 and the used manufacturing technique. These restrictions act as a guidance for the design by limiting the design space. The constraints are as follows:

1. The ring gear of the planetary gear is reserved for the novel ring actuator.
2. The output step size as results of the ring actuator should be 0.5 mm.
3. The output step size as results of the rotary actuator should be 4 mm.
4. The maximum diameter of the actuator ring is set to 70 mm.
5. The minimum sun gear and pinion diameter is 10 mm [3]
6. The spindle should meet standard thread sizes and have a maximum lead of 10 mm to be effective.
7. The minimum pitch of the ring actuator teeth is 3 mm for printing it with *PLA* [2].
8. The minimal tooth width of the ring actuator is 10 mm to withstand the external forces.
9. All materials, included bolts, nuts and bearings, need to be MR-Safe.

3.3.2 Planetary Gear

The planetary gear is responsible for the power transmission from the actuator to the output of the system. A basic planetary gear configuration is used because it features an efficient and low volume design [39]. The latter enables us to create a narrow design.

The relation between the inputs and output of the planetary gear are given by the following equation:

$$\omega_{\text{out}} = k_1\omega_1 + k_2\omega_2 \tag{3.1}$$

where $\omega_{\text{out}}, \omega_1, \omega_2$ are the angular velocities of respectively the output shaft, ring actuator and the rotary actuator. The constants k_1, k_2 are the transmission ratios between the actuators and the output shaft.

A difference with a factor of 8 is required between the two actuators to obtain the step size of 0.5 mm and 4 mm (velocity of 40 mm/s at a frequency of 10 Hz), thus in short $k_2\omega_2/k_1\omega_1 = 8$.

The transmission ratios of the planetary gear can be derived by the geometrical constraints between the gears. The basic equation for a gear is:

$$D = N \cdot m \tag{3.2}$$

[2] Magic number: A constant numerical value hard-coded in the code or design which could be replaced with named constants.

[3] If the pitch is too small the teeth will not reach an infill of 100 % due to the nozzle size and accuracy of the printer. This results in weak and fragile teeth.

	Input	Input (fixed)	Output	Transmission ratio (k_i)
1.	Sun	Carrier	Ring	$-1/\alpha$
2.	Sun	Ring	Carrier	$1/(1+\alpha)$
3.	Carrier	Sun	Ring	$(1+\alpha)/\alpha$
4.	Carrier	Ring	Sun	$1+\alpha$
5.	Ring	Sun	Carrier	$\alpha/(1+\alpha)$
6.	Ring	Carrier	Sun	$-\alpha$

Table 3.4: Transmission ratio of the planetary gear in the six possible configurations, where $\alpha = N_r/N_s$ (N_r and N_s are number of ring- and sun gear teeth)

where N is an integer representing the number of teeth of the gear and m gives the module of the gear. In order to mesh, the module needs to be equal for all the gears. To get compact design, the number of teeth of a gear should be low as possible, since it is proportional to its diameter.

The ratios for k_1 and k_2 are presented in Table 3.4. Each fundamental planetary gear train always has 4 positive and 2 negative transmission ratios, depending on the input, fixed and output configuration. To derive these ratios, one input element needs to be fixed to the real world, in other words $\omega = 0$.

The relation between the input and output torque of a planetary gear is derived from the principle of power conservation. It has an inverse relation with the ratios presented in Table 3.4. The output torque for two inputs is as follows:

$$\begin{aligned} P_{\text{out}} &= P_1 + P_2 \\ T_{\text{out}} &= \frac{T_1\omega_1 + T_2\omega_2}{\omega_{\text{out}}} \end{aligned} \tag{3.3}$$

Substitute Equation 3.1 for ω_{out} results in:

$$T_{\text{out}} = \frac{T_1\omega_1 + T_2\omega_2}{k_1\omega_1 + k_2\omega_2} \tag{3.4}$$

The relation between input and output torque per actuator can be described as follows:

$$T_{\text{out}} = k_1^{-1} \cdot T_1 \tag{3.5}$$

$$T_{\text{out}} = k_2^{-1} \cdot T_2 \tag{3.6}$$

The proposed design for the planetary gear is presented in Figure 3.4. As explained in the introduction of this chapter, the rotary actuator is connected to the carrier to create the coarse movement, whereas the ring actuator is attached to the ring gear to create the fine movement. The ring gear meshes with the planet gears, which, on their turn, mesh with the sun gear. A carrier is used to keep the planet gears in place. To reduce backlash between the gears, an involute profile is used for the tooth curvature, which gives a continuous surface contact between the gears.

The ring gear has a diameter of 44 mm, together with a module of 1, this results in a number of teeth of $N_\text{r} = 44$. The maximum number of planet gears are used to minimize the load on each gear mesh by dividing the power over multiple gears [39]. This results in number of teeth for the planet gears of $N_\text{p} = 14$. As result of the geometrical constraints of the planetary gear, the number of teeth for the sun gear is $N_\text{s} = 16$. The transmission ratio for the two actuators on the output shaft is $k_1 = 2.75$ for the ring actuator and $k_2 = 3.75$ for the rotary actuator.

Initially, this does not look like the required factor 8 as stated above. However, the rotary actuator turns more degrees per step then the ring actuator. This gives, together with the derived ratios, the required factor.

The carrier consist two parts, one that holds the planet gears by pins and has an output shaft to connect with the rotary actuator. On the other side of the planet gears, a flanged carrier is connected, to ensure that the planet gears do not slide of the pins and that the pins cannot bend when subjected to external forces. Apart from this, the flange ensures that the carrier with planet gears are aligned in the vertical plane with the ring and sun gear.

M3 nylon screws are used to connect the small plate to the carrier. The screws are sunk in the small plate, such that the screws do not protrude from the small plate. In the carrier a screw thread is tapped, so no additional nut is required. As result of both measures, the ring actuator can be designed smaller.

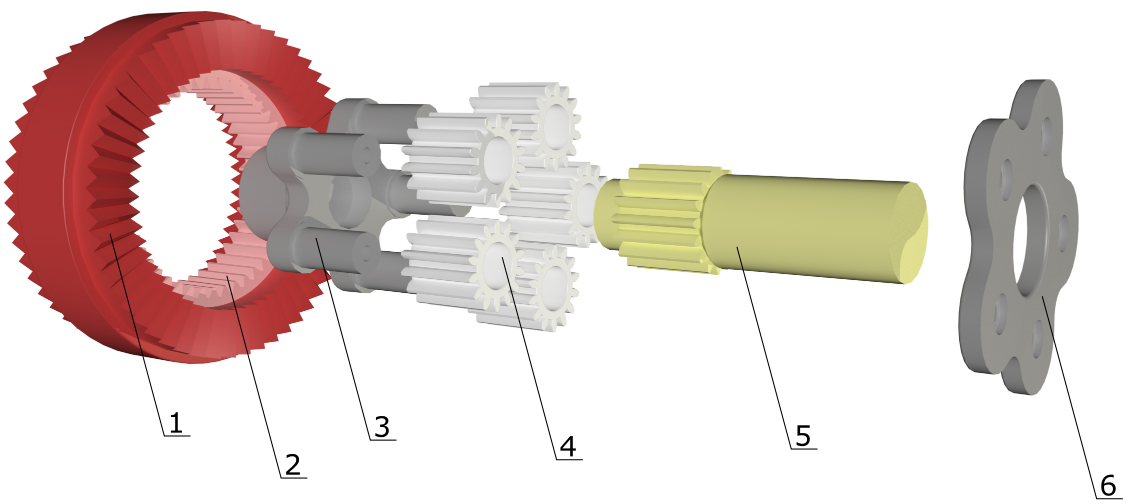

Figure 3.4: Render of planetary gear with the following parts: 1) Actuator ring; 2) Ring gear; 3) Carrier with pins; 4) Planet gears; 5) Sun gear; and 6) Flanged carrier

3.3.3 Rack-pinion

The rack-pinion is connected to the sun shaft of the planetary gear to convert the rotary output motion to a linear motion. The velocity of the rack is derived as follows:

$$v_{\text{rack}} = i \cdot \omega_{\text{pinion}} \tag{3.7}$$

where i is the ratio of the rack-pinion, which is equal to the radius of the pinion. Using power continuity, the torque on the output shaft of the planetary gear can be derived as follows:

$$T_{\text{pinion}} = i \cdot F_{\text{rack}} \tag{3.8}$$

Designing the pinion too large results in a large torque on the output shaft. In contrast, making the pinion too small creates brittle teeth and small output velocity. The rack is designed with a length of 200 mm to meet the required of 169 mm range, while leaving enough length to keep the rod aligned.

With the proposed ratios for the planetary gear, a diameter of 12.27 mm is required for the pinion. The basic gear equation 3.2 is used to determine the number of teeth of the pinion. Since the number of teeth must be an integer, and a gear module of $m = 1$ is used, the number of teeth is rounded to $N_{\text{pinion}} = 12$, so the diameter of the pinion becomes $D_{\text{pinion}} = 12\,\text{mm}$.

The pinion is the smallest gear in the actuator, and has to withhold the highest force in the rack-pinion and planetary system. The diameter of the gear, the material and its width determine the strength of the teeth. The standard equation for bending stress can be calculated with:

$$\sigma = \frac{Mc}{I_{\text{c}}} \tag{3.9}$$

Where M is the moment, c the central distance and I_c the centroid moment of inertia.

The bending stress can be derived by simplify one tooth to a single cantilever, where a force is placed at the end of the beam, parallel to the fixed world (Figure 3.5). This formula is then adjusted to specific Spur gears by adding the Lewis form factor Y and the diametral pitch P ($P = 1/m$ where m is the gear module). The altered is equation is know as the Lewis equation [40]:

$$\sigma = \frac{W_{\text{t}}P}{FY} \tag{3.10}$$

Where W_{t} is the tangential tooth load and F the face width of the tooth.

The tooth strength is calculated with a involute profile of 20°, a diametric pitch of 1, a Lewis form factor of 0.24 (derived from [40]) and PLA as material. A force of 190 N results in a minimal face width of 12 mm for the pinion.

Another potential option not discussed yet is to convert the rotary motion to a linear motion by using a spindle connected to the output shaft of the planetary gear. A spindle is better in

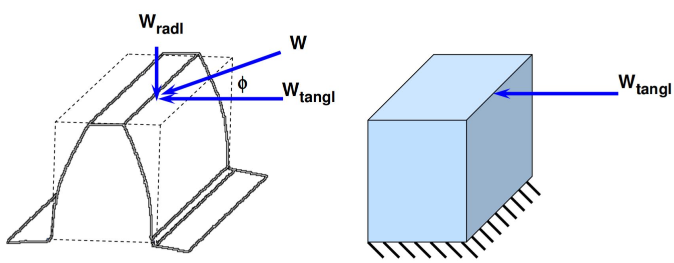

Figure 3.5: The tooth of a gear can be simplified to a cantilever, obtained from [41]

dealing with axial forces, then the rack-pinion does. However, a spindle lead of ≈ 39 mm would be required to be applied here. This is a factor ten larger then a common spindle in our type of application. Nevertheless, applying a spindle would require another gearbox to increase the angular velocity of the output, since this would decrease the spindle lead.

3.3.4 Ring actuator

The ring actuator is responsible for the fine steps and to keep the rack in position while exposed to large external forces.

The proposed design is presented in Figure 3.7, where the ring gear of the actuator is designed around the ring gear of the planetary gear [4]. These are two separate parts, but are manufactured as one solid part.

The essential of the design is based on the linear actuators presented in the research of Groenhuis and Stramigioli[5]. In his design a rack with teeth on both sides is moved by two dual-acting pistons. Each piston consists of a set of teeth on both sides. With the two pistons, four configurations can be created and are illustrated in Figure 3.6(a-d). By switching the pressure of one piston, the configuration changes, for example from (a) to (b). The rack displaces 1/4 of a step with each switch.

By alternating the pistons and switching their pressure in the presented order (a to d), the rack will move one step to the left. This sequence can be repeated multiple times to create a motion to the left. Reversing this sequence results in a movement in the opposite direction, in this case to the right.

The movement of this actuator is limited by the length of the rack. By converting the straight rack into a circular ring gear, an infinite rotary motion can be created. The diameter of the ring gear is limited by the maximum required dimension of the actuator.

The pistons are placed inside a housing. Silicon rubber seals are added behind the pistons to seal the piston chambers, since more air leakage means a reduce in effective pressure, hence less powerful actuator.

The top cover seals the pistons chamber from above. Air inlets with diameter of 3 mm are created in the top cover to fit the pneumatic hoses. Both top covers have two extending dog ears to fix the translational movement of the ring gear in the actuator. The dog ears of one of the top covers is shorter to leave space for the flanged carrier.

The top cover, housing and bottom plate are assembled together with M4 nylon screws. The bottom plate is provided with a screw thread. The housing and bottom plate are separated with the intent to create a smoother surface for the pistons to move on. This is mainly because of the manufacturing process of FDM 3D printing. The housing and bottom can be combined with other manufacturing techniques.

The ring gear has an outside diameter of 74 mm, with on each side a number of teeth of $N_{\text{actuator}} = 53$. The teeth have a width of 10 mm to withstand the piston force. Four steps are required to shift the ring gear one tooth. This results in a step size $\Delta\theta = \frac{360}{4 \cdot 53} \approx 1.7\,°/\text{step}$.

Applying the dynamic force of 90 N on the rack results in a torque of 1.5 N m on the ring gear. The static force of 190 N on the end rod results in: 3.2 N m.

The force acting on the piston generated by the air pressure is as followed:

$$F_{\text{piston}} = p \cdot A \tag{3.11}$$

where F_{piston} is the force acting on the piston, p the pressure and A the cross-sectional area of the piston. The piston is designed with a cross-sectional area of $A = 20\,\text{mm} \cdot 12\,\text{mm} = 240\,\text{mm}$.

[4]The word *ring gear* is used through out this report to address the actuator ring gear and the planetary ring gear and which one is addressed depends on the content.

At a normal operation pressure of $p = 0.5\,\text{MPa}$, this results in a piston force of $F_{\text{piston}} = 240\,\text{mm} \cdot 0.5\,\text{MPa} = 144\,\text{N}$.

The conversion from force F_{piston} to the output torque τ, acting on the ring gear, is derived with a work balance, which is as followed:

$$\tau\theta = F_{\text{piston}} x \tag{3.12}$$

where θ is the rotation caused by the displacement x of the piston. To recall, the rotation per step is $\theta = 1.7° = 0.0296\,\text{rad}$.

The displacement x of the piston is depending on the relation between the tooth pitch P_{tooth}, the pressure angle (α) of the tooth and the tooth depth (x_{tooth}). The angle of the tooth is a trade-off between tooth strength (thicker tooth) or better work transition (smaller angle). The tooth depth is derived as followed:

$$x_{\text{tooth}} = \frac{P_{\text{tooth}}/2}{\tan(\alpha)} \tag{3.13}$$

The tooth pitch is divided by two to get the adjacent of the half of the tooth, which represents the tooth depth. The pitch of the tooth is $P_{\text{tooth}} = 3\,\text{mm}$ as presented in Section 3.3.1. The pressure angle was chosen to be 24°, resulting in a tooth depth of 3.34 mm.

Getting back to Equation 3.12, the generated output torque by the piston is given by $\tau = \frac{x}{\theta}F = \frac{x \cdot 2.4 \cdot 10^{-4}}{\theta}p$. The maximum work is achieved when pushing the piston over the full tooth length, which is a displacement of $x = x_{\text{tooth}}$. The corresponding torque which this displacement is $\tau = \frac{3.34 \cdot 10^{-3} \cdot 2.4 \cdot 10^{-4}}{2.96 \cdot 10^{-2}}p = 2.73 \cdot 10^{-5} \cdot p$. With a pressure of $p = 0.5\,\text{MPa}$, the torque will be $\tau \approx 16.4\,\text{Nm}$.

However, the right piston in Figure 3.6(a) shows that the piston cannot use the full tooth depth. The misaligned is required for the working of this stepper motor, otherwise the motor will not rotate. The right pistons creates a $\pm 90°$ shift, which is 1/4 of the tooth pitch. This is exactly halfway the tooth, and this means that the displacement of the pinion is equal to the half of the tooth depth. The corresponding output torque is $\tau = 2.73 \cdot 10^{-5}/2 \cdot p = 2.73 \cdot 10^{-5}/2 \cdot p = 1.36 \cdot 10^{-5} \cdot p$. With a pressure of $p = 0.5\,\text{MPa}$, the output torque is $\tau = 8.2\,\text{Nm}$. This is the ideal situation with friction neglected.

The actual friction between the moving parts needs to be determined experimentally, however the effect of the friction can be estimated with the efficiencies achieved in the research of Groenhuis and Stramigioli[5]. The lowest efficiency achieved in this research was 50%. Taken this into account, the actuator provides an output torque of $\tau = 8.2\,\text{Nm} \cdot 0.5 = 4.1\,\text{Nm}$ at a pressure of $p = 0.5\,\text{MPa}$. This is a factor 1.3 larger then the required torque for the static force, and a factor 2.7 larger then required torque for the dynamic force.

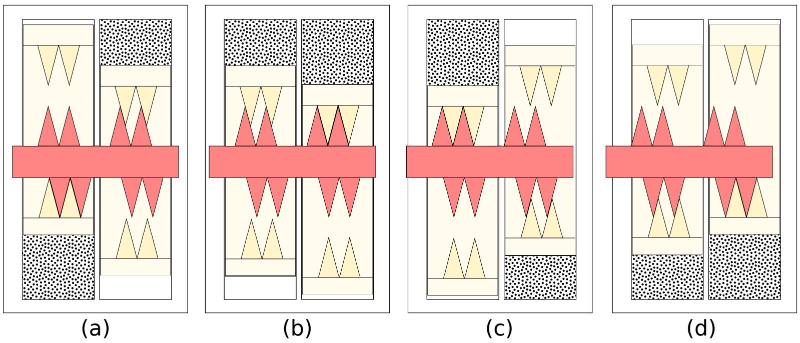

Figure 3.6: The actuator has four possible states. By following the order from left to right the rack moves to the left. Reverse that order and a movement to the right is created.

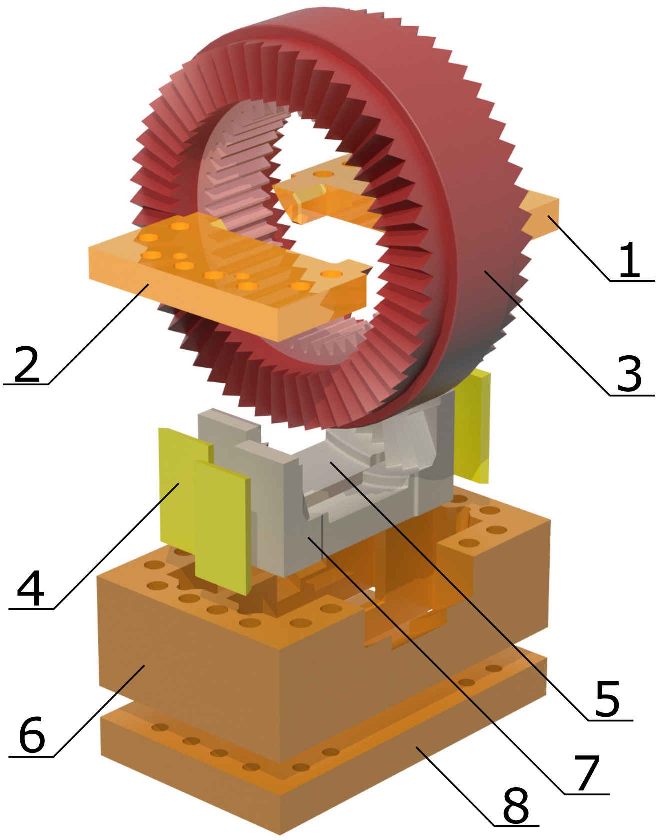

Figure 3.7: Render of the ring actuator with the following parts: 1) Top cover with long dog ears; 2) Top cover with short dog ears; 3) Ring gear; 4) Silicon seals (all yellow parts are seals); 5) Piston; 6) Housing; 7) Piston; and 8) Bottom plate

3.3.5 Rotary actuator

The rotary actuator adds coarse steps to the system. The large steps create the required high velocity output.

The rotary actuator needs to deliver at least 2.1 N m to rotate the carrier against the dynamic force. A torque of 4.4 N needs to be withstand when the static force is applied.

The R-80, a pneumatic MR Safe rotary actuator designed by Groenhuis and Stramigioli, is used as the fitting actuator [5]. A render of the design is presented in Figure 3.8. This actuator is capable to rotate at a maximum torque of 3.7 N m. How much the actuator can hold statically is not reported by the author, but after a personal communication with the author, it is presumed to be larger then the calculated required torque.

The actuator is modified to fit the socket of the carrier. The output shaft is enlarged; and the diameter of the output shaft is scaled down to 15 mm to match with the available off-the-shelf MR Safe ball bearings.

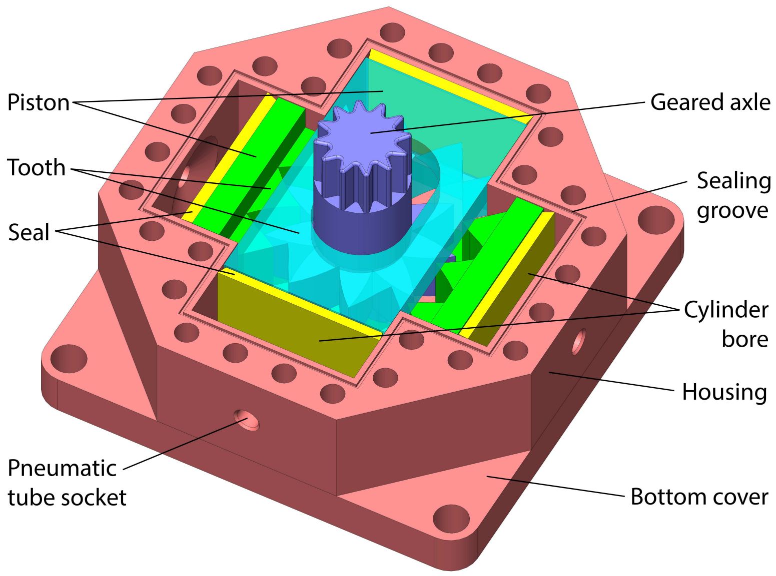

Figure 3.8: Rotary actuator R-80, obtained from [5]

3.3.6 Housing

The function of the housing is to keep all the modules together. To achieve this, errors in the part dimensions, caused by the manufacturing process, are encountered in the design. For example, the ring actuator is kept in place by two small stiffeners, but is free to move parallel to the stiffeners and in the vertical direction. This ensures that the ring actuator and the planetary gear are proper aligned with the bearings in the housing. The design is presented in Figure 3.9.

By design, silicon rubbers are added below and to the side of the ring actuator for support. The thickness of the silicon rubbers depend on the actual spacing between the housing and the actuator. Eventually, the rubbers also act as a passive damper.

The shaft of the rotary actuator and the shaft of the sun-pinion are supported by two stiffeners. Radial ball bearings are fitted around the shafts to decrease rotational friction and support for radial and small axial loads. Shaft holders are added to keep the bearings into place. The top of the shaft holders are removable to ease the assembling of the actuator. In contrast with sleeve bearings, or no bearings at all, a ball bearing is temperature efficient and has low friction coefficient. The latter increases the efficiency of the actuator, since less effective force is lost to friction.

The rotary actuator is mounted to the housing with nylon screws and 3D printed spacer and threaded nut. Straight slots are created in the housing to align the rotary actuator.

The rack-pinion housing is mounted partly to the base plate and partly to the shaft holder. In both parts straight slots are created to align the housing with the pinion.

Primary, the axial loads (thrust) are absorbed by the rack-pinion housing and this housing. A beam construction is placed on top of the bottom housing to create a stiffer for torsional loads, created by the force acting on the rack-pinion housing and the pinion itself.

The base plate, stiffeners and shaft holders are designed with guides for the air tubes to guide them from the actuators to the back of the housing. This prevents the air tubes for getting wrapped up around the ring gear.

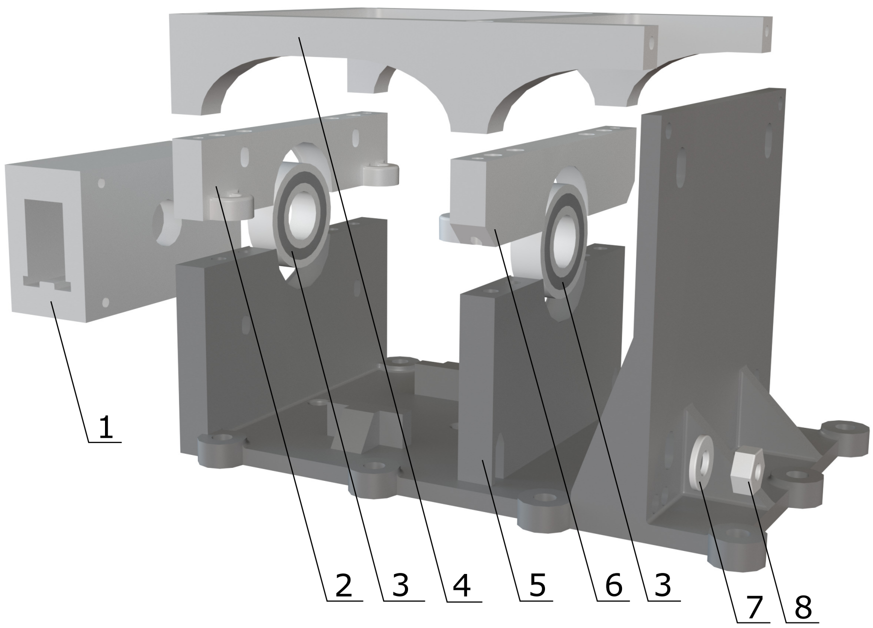

Figure 3.9: Render of housing with the following parts: 1) Rack housing; 2) Shaft holder (rack version); 3) Ball bearing; 4) Beam support; 5) Base plate with stiffeners; 6) Shaft holder; 7) Plastic spacer; and 8) Plastic nut

3.4 Realization

This section provides practical info about the realization of the actuator Firstly, it address the manufacturing of the parts. Secondly, the bought bearings are described. Lastly, the experiments with printed rubber-like material is described.

3.4.1 Manufacturing

The actuator is created with three 3D printers and a laser cutter.

The 3D printers print layer for layer, which means that the parts have a weak spot for momentum around the X and Y-axis. As the orientation has significant influence on the strength of the parts, the orientation for each part is optimized to achieve the most strength in the parts. Apart from this, the bottom layer is the smoothest layer of the part. Therefore, the pistons of the rotary motor are printed with the sliding surface down.

The base plate of the housing is printed in PLA with the Leapfrog Creatr HS 3D printer. This printer has a larger print bed, which allows to print larger parts.

The planet gears, carrier (both), ring gear, and the pistons of the ring actuator are printed in Vero transparent material with the Objet260 Connex3. This printer is able to print small parts up to a resolution of 15.9 µm. Additionally, this printer can print support material at the same time, so complex design as the ring gear can be printed.

The laser cutter is a Trotec Speedy 300 and is used to cut 8 mm thick acrylic. The top and bottom cover of the rotary motor and the bottom cover of the ring actuator are laser cutted. The pistons need to slide over these parts with lowest friction as possible. For this reason, acrylic is used for these parts since it has a smoother surface then the 3D printed parts.

The rest of the parts are printed in PLA with the Ultimaker 2. This printer is more accurate then the Leapfrog. The parts are printed in layers of 80 µm with a nozzle size of 400 µm.

The actuators are greased with Vaseline as lubrication to reduce the friction and heat of the parts. No lubrication and too tight parts result in heat which deforms the plastic.

3.4.2 Bearings

Grooved ball bearings are added to the design to reduce radial friction of the shaft with the supports. The *BB-6002-B180-10-GL* bearings from Igus are used, because these are non-magnetic and electrically insulating [42]. It uses glass balls and an in-house created material Xirodur B180 for the cage.

3.4.3 Rubber-like experiments

The ring actuator is constructed with the Ultimaker 2, but experiments are conducted to print the actuator with the Objet260 Connex3. The focus on the experiments was volume reduction, since the Objet260 can print with higher resolution and more complex designs. The designs showed potential, however the step to a smaller actuator design could not be conducted in this research.

Material	Ultimate tensile strength (in MPa)
PLA	47 - 70
Vero transparent	50 - 65

Table 3.5: Overview of the tensile strength of MR safe material and ceramic (MR compatible because of it good thermal conductivity property)

The conducted experiments are presented in Figure 3.10 and briefly explained below.

Smaller actuator Volume reduced actuators were already created in the lab, however no actuator had two separated covers (the planetary gear is placed in middle of the actuator). A prototype was created and it was validated that actuation was possible with two separated covers. The housing was designed with a full perimeter snap-on fit to mount the top covers to enable removing them later. The top covers cracked on the snap fits. Apart from this, because this printer prints only solid parts and prints soluble support, air pipes can be incorporated into the design. This gives more flexibility in the design to where to place the hoses.

Pressure test The Objet260 can print rubber-like material. It has the potential to act as a sealing for the top plate of the actuator. This experiment was conducted to examine the behaviour of the rubber under pressure. The left chamber has rounded printed seals, whereas the right one has flat printed seals. Up to maximum pressure of 70kPa was provided. In both situations of clamped and glued of the top on the chamber, no leakage was detected.

Rubber on the housing Next step was to create a design for a small actuator with rubber printed on it. The design showed potential, however the rubber-like material is more fluid, which requires more support material in the printing process. This support material is also placed on the inside of the piston chambers. The support material create a rough surface, but the pistons require a smooth as possible surface.

Ring actuator with rubber The rubber was moved from the housing to the top covers, to prevent support material in the piston chambers. The actuator was tested by clamping the top covers on top of the housing. The sealing worked, no air was leaking between the top cover and the housing. On the contrary, the seal stroke in the middle caused the seals of the pistons to bend a bit which caused leakage.

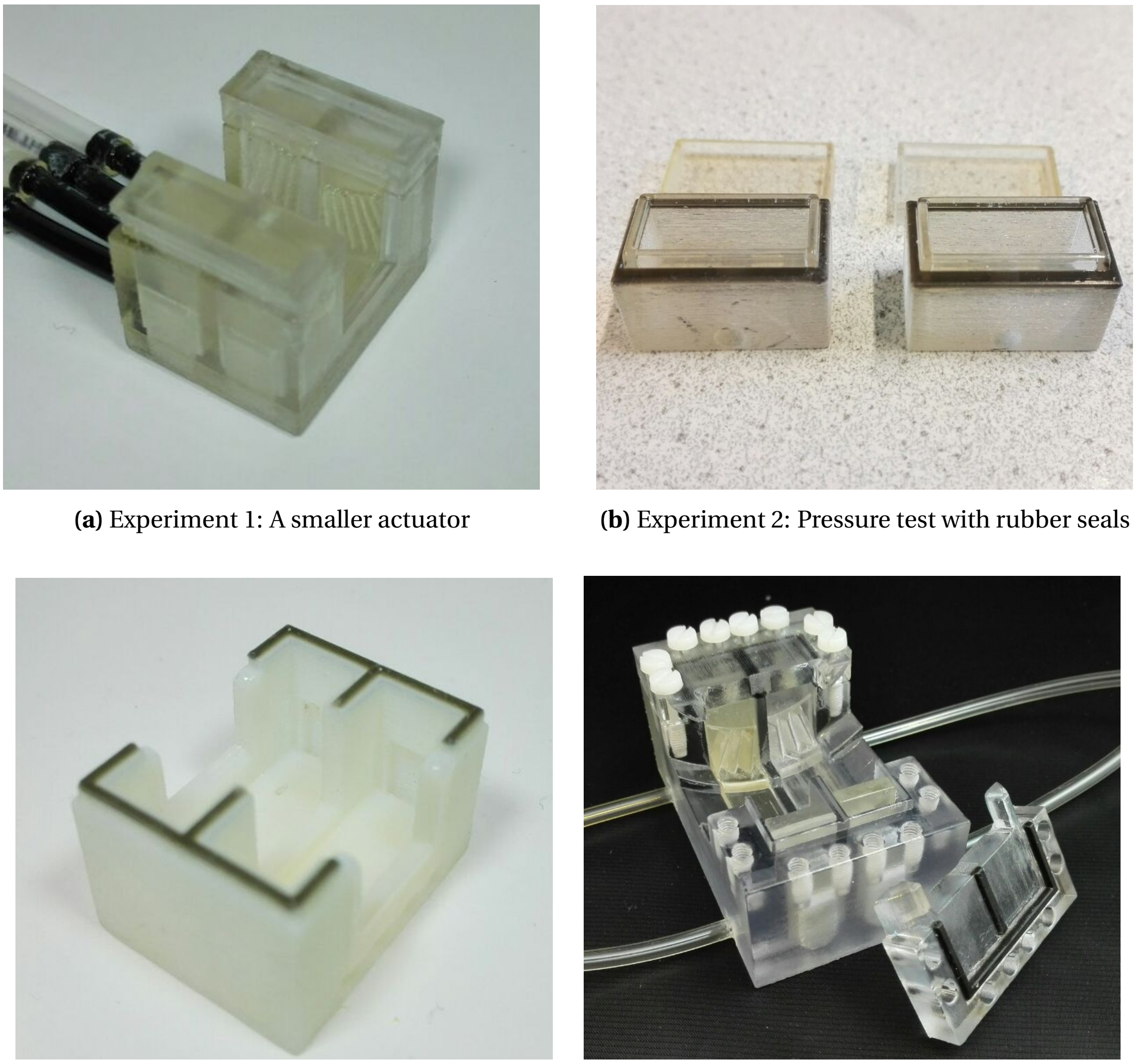

(a) Experiment 1: A smaller actuator

(b) Experiment 2: Pressure test with rubber seals

(c) Experiment 3: Rubber on the actuator

(d) Experiment 4: Ring actuator with rubber top covers

Figure 3.10: Experiments conducted with the 3D printed rubber-like material

4 Evaluation

In this chapter the proposed design is evaluated. Firstly, the equipment to control and measure the actuator is described (Section 4.1). Secondly, the conducted experiments are described (Section 4.2). The results of the experiments are presented in Section 4.3, followed by a discussion of the results in Section 4.4.

4.1 Equipment

A pneumatic driver is created to control the pistons and is presented in Figure 4.1. The driver consist of the pneumatic valves, an Arduino to control the valves and some knobs and buttons to give input to the Arduino. All the items are mounted on a piece of plastic to keep the parts together.

Four pneumatic valves, mounted on a manifold, are used to actuate both the stepper motors. Each valve controls the position of one piston. The PV5211-24VDC-1/8 solenoid driven valve is used, which has five ports and two positions. It has a working pressure of 1.5 bar to 8 bar and a switching frequency of 10 Hz. A pressure regulator is added in front of the manifold to regulate the pressure towards the actuators.

An external 24VDC 1.67A power supply is used to power the pneumatic valves. Four NPN transistors, controlled by the Arduino, switch the state of the solenoids on the valves. A 9VDC buck converter is used to downscale the voltage to power the Arduino.

An Arduino Uno with an Atmega328P-PU micro-controller is used to control the pneumatic valves. It is equipped with a proto-shield and a controller with buttons to control the actuators manually. Two analogue rotary potentiometers are connected to the Arduino to control the frequency of the actuators. The Arduino reads the analogue value of the potentiometers with 10-bit (1024) and maps it to a value between the 500 ms to 10 ms sample time, which is the inverse of the frequency. The Arduino is programmed with the Arduino IDE [43].

The Arduino is also used as data-acquisition device by sending data through its serial port. The serial port is connected by USB to a PC which runs a *Python* programme to read the data and save it to a text file. Each serial package consists of the following information in the presented order:

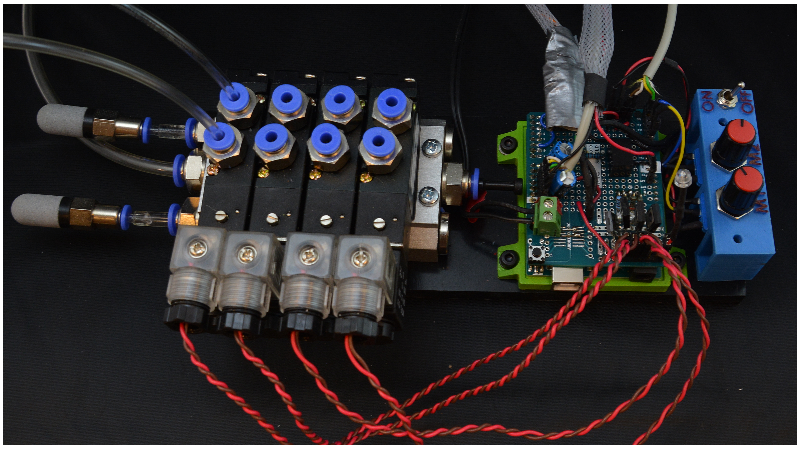

Figure 4.1: The pressure driver with four pneumatic valves, mounted on a manifold and controlled by an Arduino. The knobs in the front, together with a controller with buttons (not presented in the image), are used to control the Arduino and adjust stepping frequencies. All the parts are mounted on a black piece of black plastic to keep the parts together and prevent wire damage while moving it.

1. Elapsed time (since start measurement)
2. Position of AS5055 (10-bit)
3. Number of revolutions of AS5055
4. Value of pressure sensor 1 (10-bit)
5. Value of pressure sensor 2 (10-bit)
6. Frequency actuator 1 in sample time
7. Frequency actuator 2 in sample time

Next to the valves, the knobs, the buttons and the Arduino, a few add-ons are created to connect with the Arduino to obtain specific data.

AS5055 The first item is the magnetic rotary encoder AS5055. The range of motion of the rack is limited by design, whereas the pinion can rotate infinitely. In addition, the rotation of the pinion can be used to divided the total play in play caused by the rack-pinion and play caused by the planetary gear. The number of steps and step size of both actuators determine the rotary motion of the pinion. Therefore, a magnetic rotary encoder AS5055 is used to measure the rotary motion of the pinion. The specifications of the sensor are listed in Table 4.1. It requires a magnet placed in the centre of rotation of the pinion. The AS5055 is mounted to the housing of the rack holder with a 3D printed bracket (see Figure 4.2). The accuracy of the AS5055 is depending on the error between the centre of the AS5055 and the magnet. Therefore, a cavity of the AS5055 is designed into the bracket, so the sensor is fixed and will not move or rotate during operation.

Electronic Digital Caliper The second item is a caliper. The rotation of the pinion is sufficient for most of the experiments. However, for calibration and ratio determination the displacement of the rod needs to be known. A electronic digital caliper is used to measure the displacement. The specifications of the caliper are listed in Table 4.2. The display of the caliper shows up to two decimals.

High speed digital camera A digital camera with a high speed capturing of maximum 1000 frames per seconds is used to capture the value of the caliper while moving the actuator. Furthermore, in the force measurements, the camera is placed above the actuator to capture the movement of the actuator housing.

Pressure sensor The pressure gauge attached to the pressure regulator provides a rough indication of the provided pressure, but is far from accurate. The pressure gives feedback of the pneumatic dynamics in short and long hoses. Furthermore, it provides information about the actual pressure in the piston chamber, hence the forces acting upon the ring gear.

Two Honeywell piezo-resistive silicon pressure sensors (type: 785-ABPDANN010BGAA5) are bought for this purpose and mounted on a prototyping board (see Figure 4.3). The sensor is already calibrated and its specifications are listed in Table 4.3. The full scale span (FFS) for this sensor is 10 bar. The output signal is connected to the analogue input of the Arduino for the data-acquisition.

For the experiments an accuracy of $\pm 0.1 bar$ with a sample frequency of at least 100 Hz (sample time = 10 ms) is required to make the data useful. The analogue input of the Arduino has a 10-bit resolution, which results in a resolution of 0.01 bar/bit. The resolution of the ADC [1] and accuracy of the sensor are both sufficient for the experiments. The sensors have a sufficient update frequency of approximately 1 kHz.

[1] ADC = analog-to-digital Converter

Specification	Value	Unit
Resolution	≈ 0.09	deg
	12	bit
Maximum absolute error	± 1.41	deg
	± 16	bits
Readout time	430	μsec
Interface	SPI	

Table 4.1: Specifications of the magnetic encoder AS5055

Specification	Value	Unit
Measuring Range	0-150	mm
Resolution	0.01	mm
Accuracy	0.02	mm
Maximum measuring speed	1500	mm/sec

Table 4.2: Specifications of the digital caliper used in the experiments

Specification	Value	Unit
Measuring Range	0-10	bar
Total error band	± 1.5	FFS
	± 0.15	bar
Accuracy	± 0.25	FFS
	± 0.025	bar
Maximum sample frequency	≈ 1 kHz	
Interface	Analogue	mm

Table 4.3: Specifications of the piezo-resistive silicon Honeywell pressure sensor with type-number 785-ABPDANN010BGAA5 (FFS = Full Scale Span (= 10 bar))

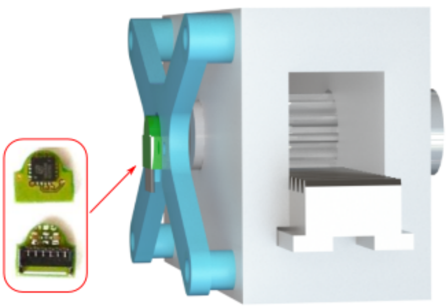

Figure 4.2: AS5055 (green part) and the bracket (blue part) connected to the white housing of the rack-pinion to measure the rotation of the pinion.

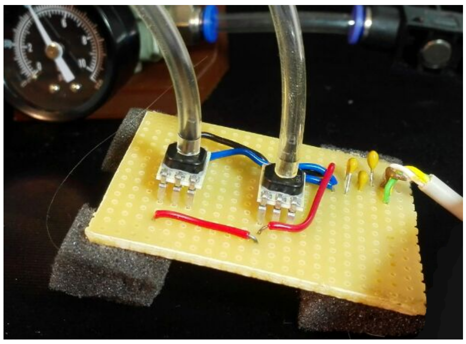

Figure 4.3: Two analogue pressure sensors mounted on a prototyping board which is connected to the analogue ports of the micro controller.

4.2 Experiments

In this section the experiments and their methods are described.

4.2.1 Step size

The caliper is used to measure the actual displacement of the rack. The caliper is rigidly attached to the lab table and the sliding part of the caliper is positioned against the rack. The AS5055 measures the actual rotation of the pinion.

The rack is moved for a range of steps and the actual displacement is measured. The data of the AS5055 sensor is used to validate that there were no steps missed. From the acquired data the step size and accuracy of the steps of both actuators can be derived. Furthermore, the actual ratios of the planetary gear and the rack-pinion mechanism can be determined.

4.2.2 Play

Pressure is applied on the actuators and a small force is applied on the rack. The caliper is used to measure the displacement caused by the limited force and the AS5055 is used to measure the rotation of the pinion.

The displacements measured by the caliper represent the total play in the system. In combination with the data of the AS5055 the contribution in play can be separated in 1) rack-pinion; and 2) planetary gear plus actuators.

4.2.3 Maximum unloaded frequency

The frequency of the actuator is increased until the actuator starts missing steps. Tubes with a length of six meter are used between the valves and the actuator. The pressure sensors are both connected to the same tube. One pressure sensor is positioned directly after the valve and the other just in front of the actuator.

The experiment validates the output velocity of the actuator. Next to that, it identifies the time delay caused by the long hoses. By conducting the experiment with both actuators, it is possible to map the difference between the actuators, since they differ in piston chamber volume.

4.2.4 Force versus pressure

The weight is increased in steps of 1 kg until the actuator cannot lift the weight any more without missing steps. Then the pressure is increased and the weight-adding is repeated. The starting pressure of this experiment is where the actuator can barely move without any load. This test ends at a maximum pressure of 5 bar or if the actuator gets damaged.

The set-up to lift the weight is presented in Figure 4.5. The actuator is connected via a rope along a pulley to a mass. The mass starts at the ground and the actuator lifts the mass in the air.

From this data the dynamic force of the actuator can be extracted.

4.2.5 Force versus speed

The frequency of the actuator is increased until the actuator starts missing steps. Then the weight is increased with 1 kg and the test is repeated. The test will repeat itself until the weight is found where the actuator cannot move on the lowest frequency. The actuator is connected with short hoses (0.5 m) to the valves. The same set-up as in the previous experiment is used.

The data of the pulling force and output speed multiplied reveals the power distribution of the actuator. In combination with the input pressure and stepping frequency, the maximum efficiency of the actuator can be derived.

4.2.6 Magnetic Resonance Imaging

In this experiment the effect of the actuator on MR images is measured. A female breast phantom is used to mimic human tissue under the MR scanner.

The manifold with solenoid valves and Arduino are required to control the actuator. However, these parts are made from metallic and emit RF-signals caused by the electronics, so it is unsafe to place them inside the MR scanner. A cage of Faraday is build around the scanner to create a safe and interference free area inside the cage. The unsafe components are placed outside the cage and the valves are connected to the actuator with 8 meter long hoses (see Figure 4.6). A compressor is used to supply pressure to the manifold.

The MRI experiment consists of three scenarios, which are preformed multiple times:

1. Set NA   No Actuator, phantom only
2. Set A   Phantom with Actuator, but no pressure applied on the actuator
3. Set AA   Phantom with Active Actuator

When the actuator is not MR safe because of metal parts, a bright spot on the image at the metal position is expected. Next to that, a disruption in form of ringing around the metal occurs. When the actuator consist of electrical components, then a bright straight line is expected on the image. Typically, electrical components emit at one frequency which is one single point in the frequency domain of the image. This single point results in a straight line across the image. The direction of the line depends on the phase of the signal.

The effects of metal and electronics in MRI are discussed, but what is expected when the actuator is 100 % MR safe? Since it is not going to emit RF signals and does not contain any magnetic and conducting parts, it will simply not be visible on the MR images. In order to know where the actuator is positioned on the MR images, fish oil markers, which are captured by the MR scanner, are placed on the actuator. The markers are position in different orientations, which makes it easier to determine the orientation of the actuator on the MR image.

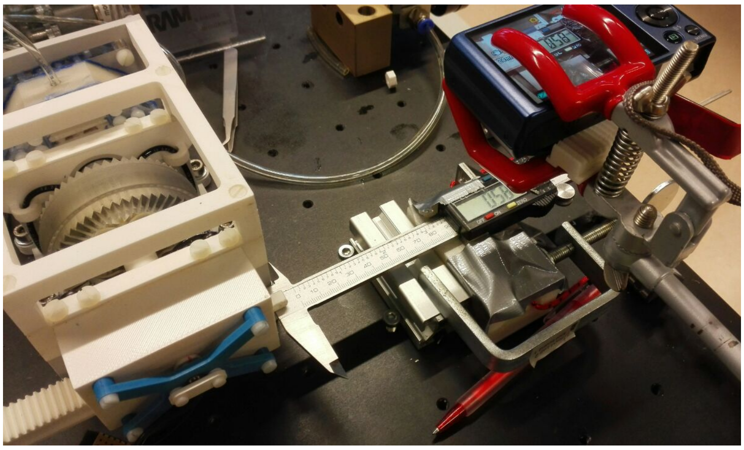

Figure 4.4: The digital caliper is mounted to the lab table. The sliding part of the caliper is placed against the rack. A camera is mounted above the caliper to log the values on the caliper.

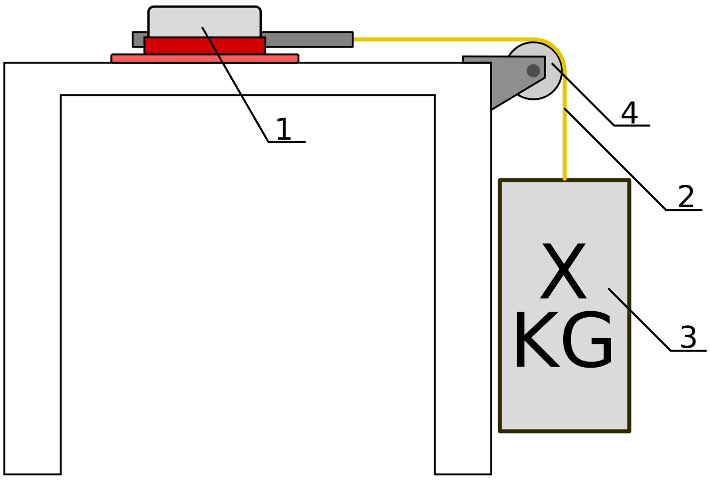

Figure 4.5: Force set-up where the actuator (1) is connected with a rope (2) to a mass (3). A pulley (4) is used to guide the rope to the horizontally placed actuator. The actuator is mounted on the lab table

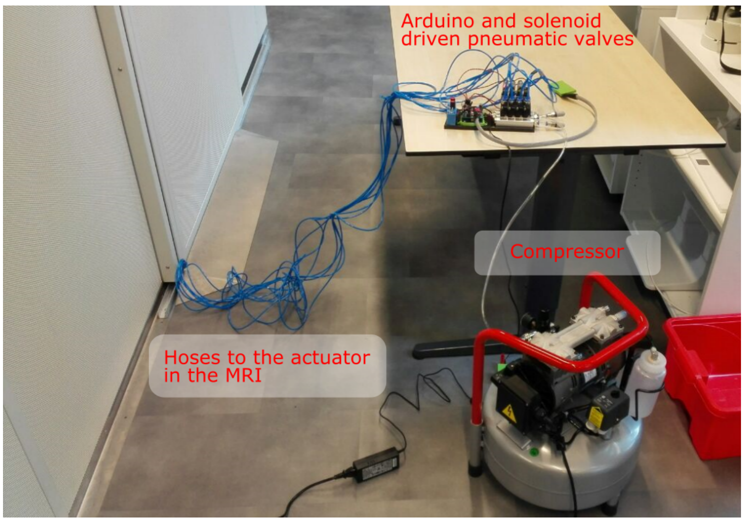

Figure 4.6: The pneumatic set-up to control the actuator in the MRI. The door of the MRI is slightly open to provide an entrance for the hoses to the actuator.

4.3 Results

This section demonstrates the results obtained in the experiments in the same order as the previous section.

4.3.1 Step size

The results of this experiment are listed in Table 4.4. Four measurements are conducted per actuator. The displacement (or shift) per measurement is given, together with the total number of steps and rotation of the pinion. With the data of these three parameters, the displacement and rotation of the pinion per step is calculated. The planetary gear ratio is calculated as followed

$$i_{\text{rcs}} = \frac{\theta_{\text{tot}}}{S \cdot \theta_{\text{ring}}} \tag{4.1}$$

$$i_{\text{crs}} = \frac{\theta_{\text{tot}}}{S \cdot \theta_{\text{carrier}}} \tag{4.2}$$

where θ_{ring} and θ_{carrier} are the rotary displacement of the ring gear and carrier per step ($\theta_{\text{ring}} = 360/(53 \cdot 4) \approx 1.67°$ and $\theta_{\text{carrier}} = 10°$). The pinion radius is calculated as followed

$$i_{\text{pin}} = \frac{x_{\text{tot}}}{\theta_{\text{tot}}} \tag{4.3}$$

The results of the second measurement of the ring actuator are presented in Figure 4.7. Figure 4.7a gives the relative position of the pinion, where the deviation from the mean per step is displayed in Figure 4.7b. During the measurement the revolution counter updated, which caused missing data for a time span of 250 ms. As result, one step is not logged, but the data is rectified for the missing step to not affect the mean and standard deviation.

The measured rotation per step results in a mean of 0.080 rad with a standard deviation of 0.009 rad. The maximum deviation of ±0.0276 rad was measured. A mean step size of 0.489 mm with a standard deviation of 0.002 mm is achieved. The standard deviation represents the distribution of the step size around the mean. A high value means that the numbers a spread out, whereas a low value means the values are close to the mean value.

The sensor has a resolution of 12-bit, however due to an error in the data-acquisition code, the resolution downgraded to 10-bit. Consequently, the 10-bit downgrade gives a resolution for 1LSB of 0.0061 rad (or 0.0368 mm (calculated with a pinion radius of exactly 6 mm)).

The results of the second measurement of the ring actuator are presented in Figure 4.8. Figure 4.8a gives the relative position of the pinion, where the deviation from the mean per step is displayed in Figure 4.8b. The actuator performs the larger steps, therefore the number of steps per measurement possible in the measurement is a factor eight less then the ring actuator. The measured rotation per step results in a mean of 0.654 rad with a standard deviation of 0.031 rad. A maximum deviation of ±0.0706 rad was measured. A mean step size of 3.924 mm with a standard deviation of 0.016 mm is achieved.

The factor between the ring- and rotary actuator is derived with both mean step sizes, and results in a factor of 8.02 An average of 6.05 mm is obtained for the radius of the pinion.

4.3.2 Play

Figure 4.9 shows the results of the play measurement. In total five measurements are performed and in between each measurement the rack is moved to a different position. The caliper was only proper constraint in one direction, therefore only in the direction towards the weight is measured.

The mean displacement of the rack is 0.68 mm with a standard deviation of 0.09 mm. The results of the pinion are multiplied by the radius of the pinion to compare the results with

Actuator	Exp. #	Shift rack x_{tot} (mm)	# of steps S	Rotation pinion θ_{tot} (rad)	Shift per step x_{step} (mm/step)	Rotation per step θ_{step} (rad/step)	Planetary ratio i_{rcs} / i_{crs}	Pinion ratio i_{pin}
Ring actuator	1	23.05	47	3.731	0.490	0.079	2.68	6.18
	2	51.29	105	8.450	0.488	0.081	2.72	6.07
	3	55.57	114	9.173	0.487	0.081	2.72	6.06
	4	52.17	107	8.590	0.488	0.080	2.71	6.07
Rotary actuator	1	51.15	13	8.525	3.935	0.656	3.76	6.00
	2	50.86	13	8.517	3.912	0.655	3.75	5.97
	3	51.24	13	8.529	3.942	0.656	3.76	6.01
	4	54.73	14	9.093	3.910	0.650	3.72	6.02

Table 4.4: The step size results of the ring- and rotary actuator and the corresponding derived transmission ratios

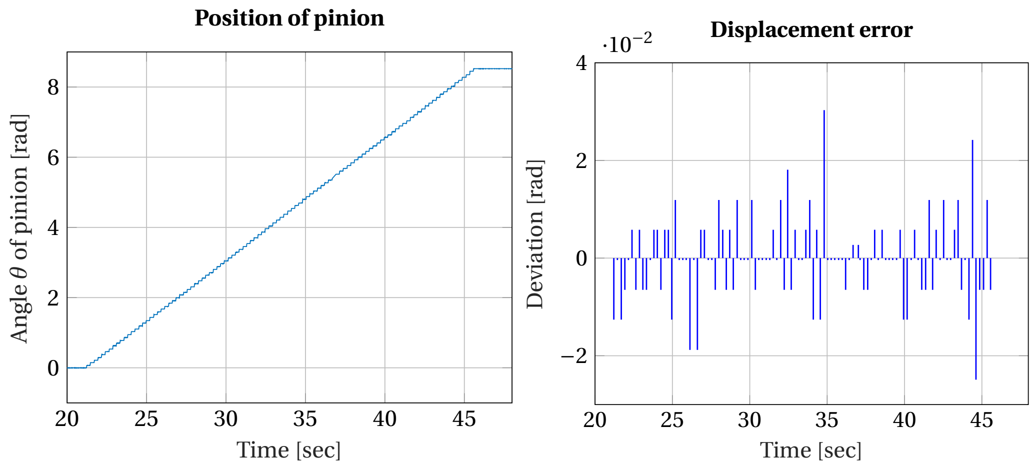

(a) Position of the pinion in rad

(b) Deviation of the mean per step

Figure 4.7: Step size results for the ring actuator of the second measurement

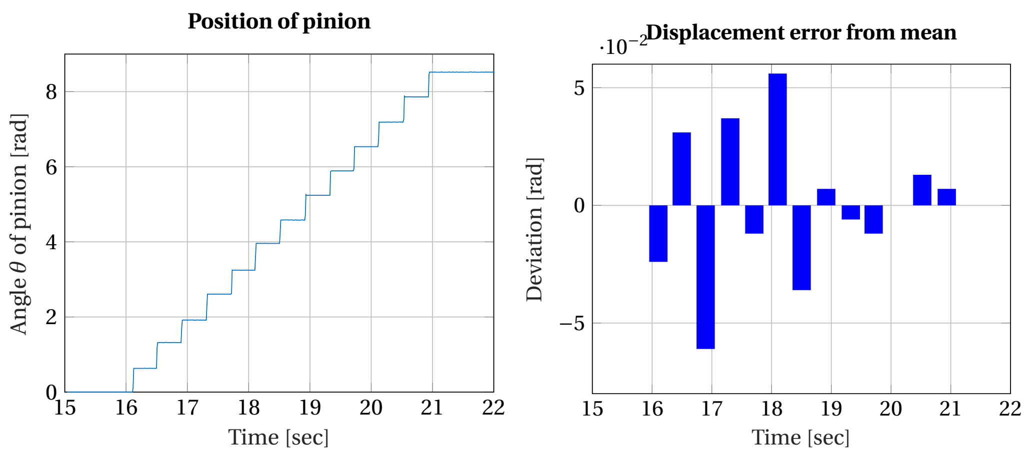

(a) Position of the pinion in rad

(b) Deviation of the mean per step

Figure 4.8: Step size results for the rotary actuator of the first measurement

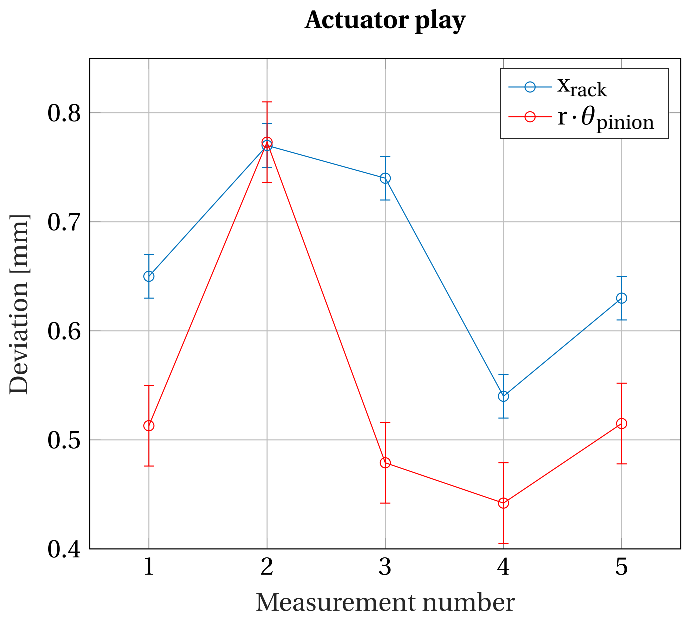

Figure 4.9: Play measured on the rack and pinion (multiplied by $r_{pinion} = 6\,\mathrm{mm}$)

the same unit. The pinion has a mean displacement of 0.54 mm with a standard deviation of 0.13 mm.

4.3.3 Maximum unloaded frequency

The maximum unloaded stepping frequency of the ring actuator is displayed in Figure 4.10. A maximum frequency of 23 Hz is found at 0.22 MPa. Two fast switching Festo valves are used to validate that the maximum frequency was indeed limited by the actuator and not by the maximum switching frequency of the pneumatic valves.

Figure 4.11 presents the maximum unloaded stepping frequency of the rotary actuator. The rotary actuator has a maximum frequency of 18 Hz. As result of changes in the settings of the experiment, the pressure was increased towards 0.31 MPa.

4.3.4 Force versus pressure

Figure 4.12 presents the results with the rotary actuator. The rotary actuator lifted a load of maximum 90N with a pressure of 2.9 MPa. At 100N, the actuator starts missing steps and the actuator could not lift the weights any more.

The experiment was stopped at this pressure, because the layers of the housing started to split at a crucial place in the housing under the load of 100 N. The crack is shown in Figure 4.13.

A linear function is fitted on the data and resulted in:

$$F_{\mathrm{fit}} = 393.9p - 24.2 \tag{4.4}$$

where p is the applied pressure in [MPa] at the actuator and F_{fit} the estimated force in [N].

The ring gear was already damaged in this experiment, caused by the experiment in Section 4.3.5, therefore no experiments with the ring actuator were performed. The ring actuator was able to lift 40 N in the force versus velocity experiment before the teeth broke down.

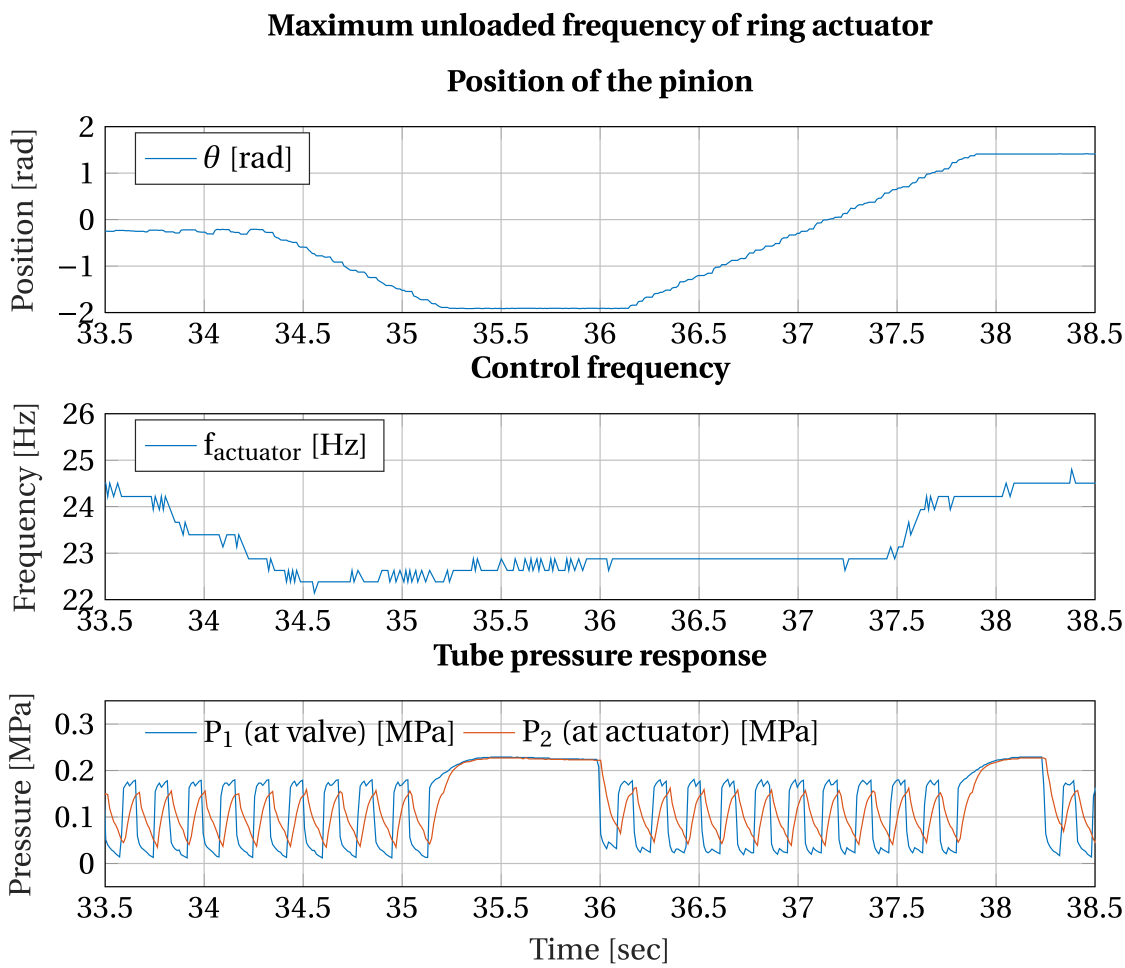

Figure 4.10: Maximum frequency of the ring actuator at 0.22 MPa is approximately 23 Hz)

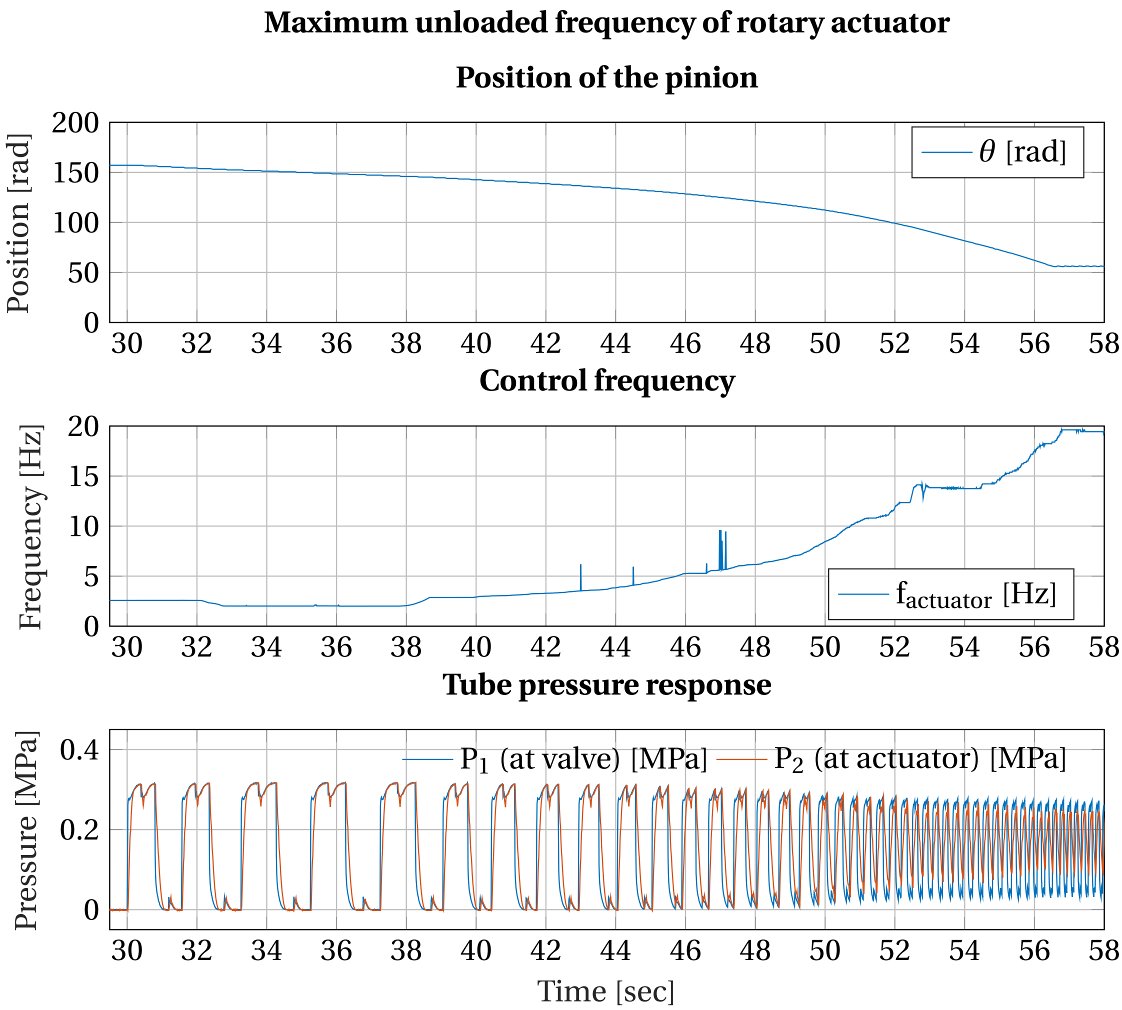

Figure 4.11: Maximum frequency of the rotary actuator at 0.31 MPa is approximately 18 Hz)

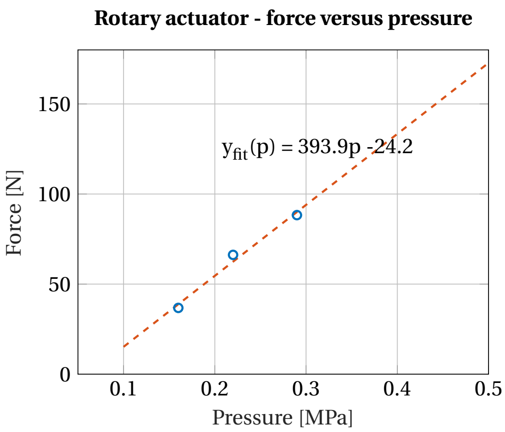

Figure 4.12: Force versus pressure results for the rotary actuator

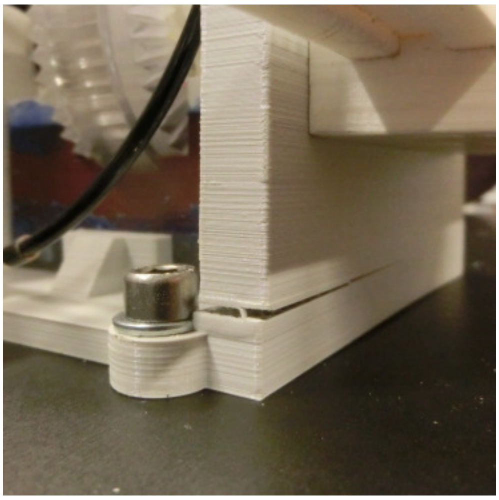

Figure 4.13: Crack between the layers of the housing when 100N is applied on the rack.

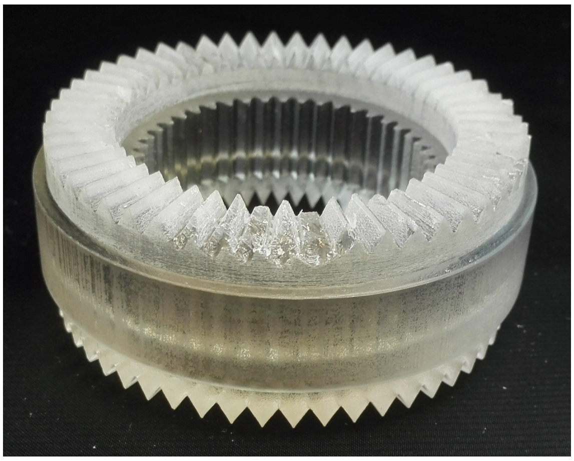

Figure 4.14: Broken teeth of the ring actuator gear

4.3.5 Force versus velocity

This measurement aimed to obtain the power specifications of the actuator with maximum speed in normal operation range. Therefore, the pressure in the piston chambers was increased to 0.5 MPa.

During the preparation of this experiments the ring actuator started to malfunction. The actuator was jammed. After de-assembling the ring actuator, several teeth of the ring actuator gear where broken (see Figure 4.14). The broken parts got between the teeth of the piston and the ring gear, which caused the jamming. Because of this, no further results are obtained in this experiment.

4.3.6 Magnetic Resonance Imaging

The phantom and actuator are scanned with 3D Hyce scan. This results in a multilayer 3D image of the objects under the coil. A scan consisted of 214 slices of each 0.45 mm thick. The *Partial Fourier* was set to 65% and the Number of series was set to 2, to reduce the scan-time without significant increase of noise on the MR image. A quality factor of 71 was achieved.

The breast phantom is placed in the centre of the RF-coil, which is located in the middle of the MR scanner. The actuator is placed against the breast phantom (see Figure 4.15a). The

RF-coil captures the RF signals emitted by the phantom and actuator. The largest RF-coil (coil 20) is used to capture as much signal as possible, because of the relative large dimension of the actuator.

In the preparations, fish-oil markers where placed on top of the actuator. However, this area was out of the RF-coil range (see Figure 4.15b). The maximum height is calculated by multiplying the number of slices with the slice thickness, which results in a maximum height of 96.3 mm. The markers where placed on the bottom plate of the actuator housing to be in the measurement range.

In total 14 scans were performed, where 8 scans were eventually adequate for analysing. Figure 4.16 shows a set of scans, each representing one scenario at the same scan height. The markers on the actuator are visible in the left corner on the second and third image. The actuator is not visible nor creates ringing at the breast around the markers. The breast itself shows some degradation due to the so called Gibbs artefact, but this is caused by the finite resolution for the Fourier transform to reconstruct the MR signals into an image [44].

A bright line was detected in the scans. This bright line was visible in all scenarios and is shown in Figure 4.17. This is an artefact, also known as Zipper artefact, which is caused by RF noise created by electronic devices [44]. Firstly, the phase encoding was changed 90° to confirm this was indeed an artefact by RF noise (image c). Secondly, the actuator was removed out of the MR room (image a). The artefact appeared in both situations. To the naked eye it looks as if that Figure 4.17(a) is less affected by the artefact, however, closer inspection showed that this is not the case.

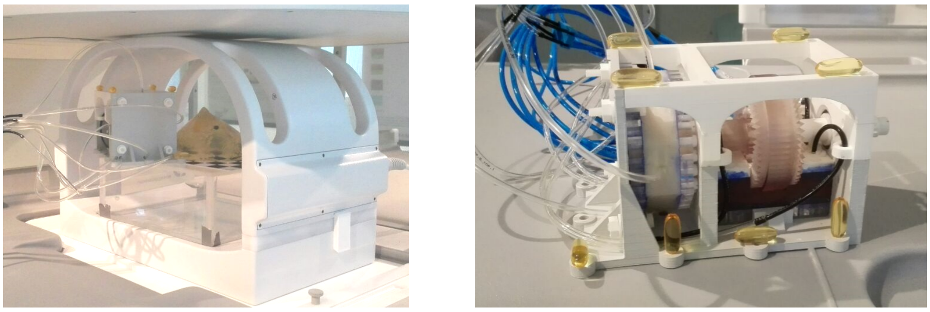

(a) The actuator placed in the MRI with the breast phantom. The markers' side of the actuator is located closest to the phantom.

(b) The actuator with the initial fish oil markers on top of the actuator and the second attempt on the bottom of the actuator. The markers are placed in different orientations to determine the position on the MR image.

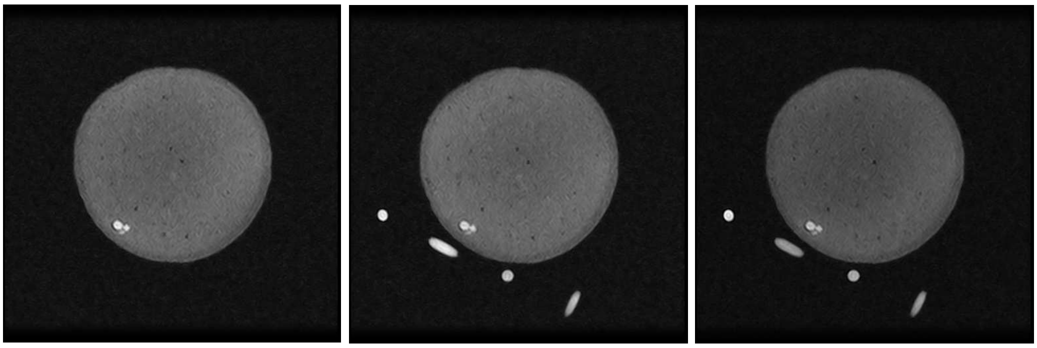

(a) Breast phantom only (NA) **(b)** Inactive actuator (A) **(c)** Active actuator (AA)

Figure 4.16: MR scan results for each scenario. These images are captured at the same height in each scan.

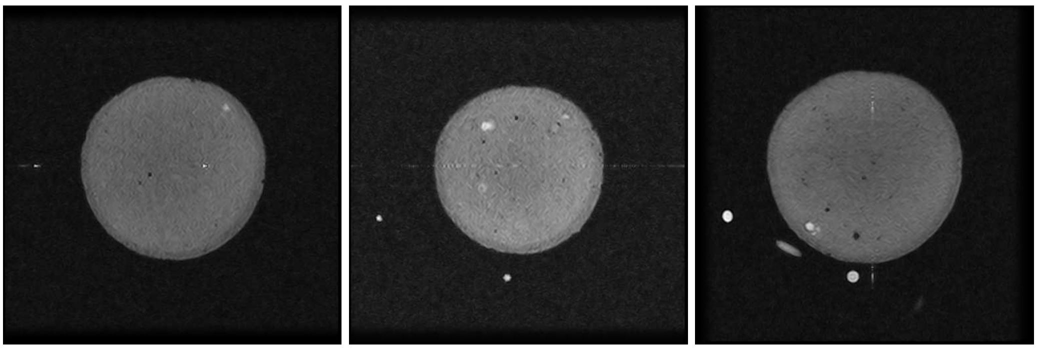

(a) Breast phantom only **(b)** Active actuator **(c)** Active actuator with 90° phase encoding

Figure 4.17: A zipper artefact is visible in all scans as a straight bright line near the centre of the image. The line is oriented in the direction of the phase encoding.

4.4 Discussion

This section starts the discussion that will aid in deriving a proper conclusion for this thesis. The requirements determined in Section 3.1 are compared with the results. Several assumptions are inserted in this section to try to find the most suitable explanation why several results differ from the expectations.

The requirements from the analysis are presented in Table 4.5. Apart from these requirements, the actuator could only be constructed from MR safe material and had to be driven with pneumatics. Each requirement is, in the same order as the table, discussed in this section.

Id	Requirement	Relation	Value	Unit	Priority
R001	Step size	$<$	0.5	mm	Must have
R002	Velocity	$>$	40	mm/ sec	Must have
R003	Static Force	$>$	195	N	Should have
R004	Dynamic Force	$>$	88	N	Should have
R005	Stiffness	$<$	0.5	mm	could have
R006	Range rod	$>$	169	mm	Could have
R007	Dimensions	$<$	$275 \times \oslash 85$	mm	Could have

Table 4.5: Requirements

4.4.1 Step size

This requirement is fulfilled with an average step size of 0.489 mm. The planetary ratio i_{rcs} was designed to be 2.75 and resulted in an average of 2.7. That is equal to a 0.3 mm increase of the sun gear, or a 0.8 mm decrease of the ring gear. In addition, the planetary ratio i_{crs} has an average of 3.75, which is equal to the ratio in the design.

The planetary gear ratios in Table 3.4 reveal that ratio $i_{\text{crs}} = i_{\text{rcs}} + 1$. However, the difference between the two ratios is 0.95. To compare, this is equal in an increase of 0.1 °/step on the output shaft of the rotary actuator. Further investigation, especially measuring the output shaft of the rotary actuator, would give more information to explain the difference in the ratios better.

The position accuracy of the rack is estimated to calculated the position accuracy of the needle. The position accuracy of the rack depends on the accuracy of the ring actuator and the rotary actuator. Combining the maximum step deviation of both actuators and multiply it with the average pinion radius results in a total position error of $\Delta x_{\text{rack}} \approx (0.0276\,\text{rad} + 0.0706\,\text{rad}) \cdot 6.05\,\text{mm/rad} \approx 0.59\,\text{mm}$. Using the ratio for the worst case position, derived in Section 3.1, the position error of the needle on the manipulator is $0.59\,\text{mm} \cdot 1.46 \approx 0.86\,\text{mm}$. This is within the accuracy of 2 mm, which means the accuracy of the actuator is sufficient in this case.

4.4.2 Velocity

The initial thought was that the stepping frequency of the actuator would be limited to 11 Hz for 6 m long hoses. This still holds for each valve, but combined, the maximum frequency can be boost up to 22 Hz for the ring actuator and 18 Hz for the rotary actuator.

This means that the actuator with a step size of 3.924 is able to achieve a maximum velocity of 70.6 mm/ sec, which is almost twice as fast then the required velocity. It is an increase of more then a factor 3 compared with other designs [5, 4]. To put it in other words, the actuator could be constructed with a smaller planetary gear ratio, up to a reduction of 2.3 mm step size for the course actuator.

4.4.3 Static & Dynamic force

Multiple teeth of the ring gear were broken off and many were damaged by the *force versus velocity* experiment. As observed in the results of the experiment, the actuator stopped working before the experiment was started. An explanation why the teeth of the ring gear broke off is given in the *Broken teeth* paragraph below.

The rotary actuator was able to move a force up to 90 N at a pressure of 2.9 MPa, which equals the dynamic force requirement.

A linear fit of the measurement data was presented in Equation 4.4. When using the actuator under a the normal operating pressure of 0.5 MPa. The dynamic force is estimated to be 173 N.

However, the housing got damaged while lifting a load of 90 N and resulted in an early stop of the experiment. An inspection of the damage is conducted and discussed in the *Broken housing* paragraph below. Since the housing was damaged as result of this test, and not the actuators, it cannot be said if the actuators can lift the estimated dynamic load under the normal pressure. Furthermore, the static force could not be validated and therefore unknown if the actuators could hold this force.

To summarize, the proposed actuator holds the dynamic force successfully, but with the current housing design this is the limit, thus it failed to hold the static force.

Broken ring gear In Figure 4.18, one of the two pistons is displayed in two configurations. Under *Normal conditions*, the direction of the second piston (not displayed) is changed before the meshed pistons changes. Then, when the first piston changes, the ring gear shifts to the right and the piston teeth ends at the half of the ring gear teeth. Next, the second pistons changes again and piston one moves the ring gear and meshes perfect.

When the actuator is operating *beyond its maximum frequency*, the first pistons moves too fast after the second piston moves. As a result, the second piston could not transmit its power and move the ring gear. Because of this, the first pistons hits the ring gear at the tip of the teeth, which are the most vulnerable parts of the ring gear and the pistons.

Operating beyond the limit was tested at lower pressures. The piston are less powerful and heavy damage was preserved. But, for the force versus speed test the pressure was increased to the normal operating pressure of 0.5 MPa. As shown in Equation 3.11, the force of the pistons increase proportional with the pressure increase. In the preparations, the maximum frequency was exceeded multiple times at the normal operating pressure to tune the code in the micro controller.

Apart from this, the print process plays an important part in the smoothness and beauty of the printed part. The ring gear is printed solid with a glossy surface (see top picture of Figure 4.19). Support material is used during the print process of the ring gear, because it is a complex part to print. This support material leaves residues on the ring gear, which can be removed partly by polishing. Experience learned that parts of the objects that are surrounded with support material are more brittle then without the support material. The adhesion in the core material is poor and some cracks are visible in the teeth (see bottom picture of Figure 4.19). The tooth that broke of was on the weaker side (the bottom picture) of the ring gear.

To conclude, the increased pressure, weaker teeth and operating too many times above the maximum frequency has led to a broken tooth. In all probability, the broken particles of the tooth fell between the piston and ring gear and caused damage on the other teeth when the piston moved towards the ring gear.

Broken housing The shaft holder of the pinion is partially broken off the housing due to the forces in the force versus pressure experiment. The split between the two parts is visible in Figure 4.13.

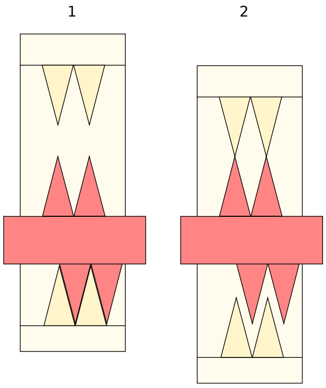

Figure 4.18: Teeth clash occurs when the piston (yellow part) meshes with the side teeth of the ring gear (red part) (1) and changes direction while the ring gear does not move (2)

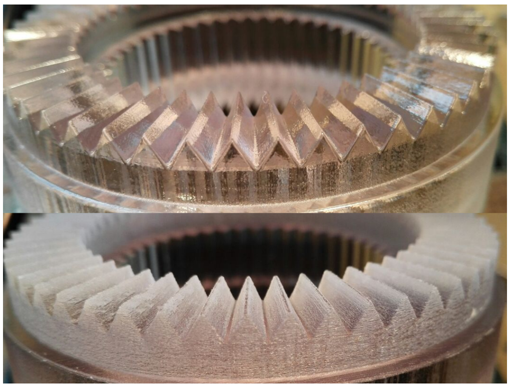

Figure 4.19: The ring gear is printed with a glossy surface (top figure), but requires suppport, which leaves a residue on the surface (bottom figure). Cracks in the teeth are visible on the teeth at the left side of the bottom figure.

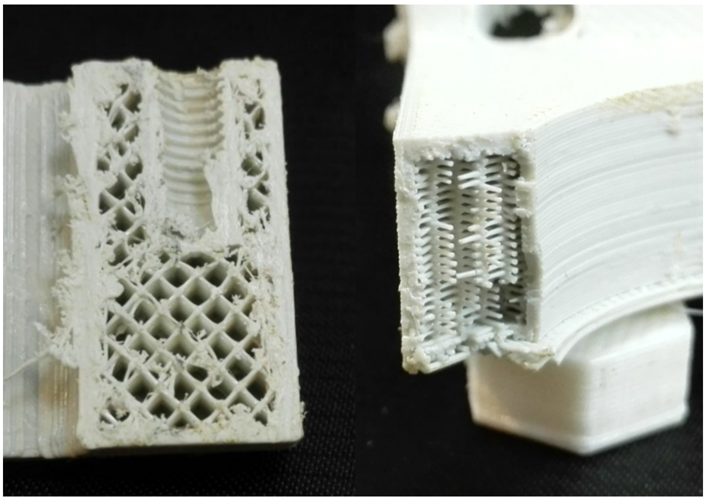

Figure 4.20: Sample of housing print batch, showing the infill structure at 25% print

Two decisions during the print process caused the housing to become weaker, that is 1) the infill percentage and 2) the infill pattern. To reduce the print time, the infill percentage is lowered. In other words, the amount of material used is reduced. In addition, a infill pattern is used to support the shell of the object and to keep the object strong with less material.

Figure 4.20 shows on the left side a section on the horizontal plane of a part that was printed in the same print batch as the housing. A grid shaped infill pattern in both diagonal directions was used with an infill of 25%. The right side shows a section on the vertical plane of the same part The housing is printed with the pattern *Lines* by the Ultimaker 2 3D printer. The pattern prints one diagonal direction per layer.

Because of this, the layers are only connected with each other on the intersections of the diagonal lines. This creates a rather strong part in the translational directions (X, Y, Z), but a weak connection in the rotational directions. The force on the rack is captured by the pinion and the rack-pinion housing and converted to a torque which acts on the rest of the housing. Unfortunately, due to the print pattern this torque acts on the weakest direction of the housing, and compromised the layer bonding at 100 N.

4.4.4 Stiffness

In the previous experiments the housing of the actuator was broken, therefore no experiment is conducted to measure the stiffness of the actuator.

On the contrary, the play in the actuator is measured. The mean displacement measured at the rack was 0.68 mm, of which a mean of 0.54 mm was caused by the play in the actuators and planetary gear.

However, as a consequence of the large uncertainties in this measurement, no accurate division of the play between the rack-pinion and the planetary gear with actuators can be derived. These uncertainties were caused by a not proper mounted caliper; and because the pinion position was measured with 10-bit resolution.

4.4.5 Range rod

The rod is designed with a sufficient length for the range. Further research has to determine how much the rack bends when fully elongated and if this is within the limits for the manipulator.

4.4.6 Dimensions

With the current dimensions the actuator is too large to fit in the manipulator. The designs are not optimized to reduces space, because the focus was on proofing the dual drive planetary principle. The next step would be to optimize the actuators, create a circular housing and integrate the bearings with the ring actuator to reduce the total dimensions of the actuator.

4.4.7 MR category

The actuator was not visible on the scans and did not causes ringing at the side of the breast, which indicates that the actuator is created from MR Safe materials.

Multiple scan were performed with different operating conditions of the actuator. On the scans a white line was noticed in the middle of the screen, but it also appeared at the phantom only scan. This excludes the actuator from being the cause of the RF noise.

The MR images are captured in a 0.25 T MR scanner, where nowadays 3 T to 7 T is used. Using a scanner in that range would give more insight about the actuator, however since it is made from only MR Safe materials and uses pneumatic as actuation principle, the expectation is that the results would not differ much.

5 Conclusion

The aim of this reseach was to develop a MR Safe actuator with an increased output velocity, while maintaining the accuracy. Two main research questions were stated in the problem statement. In this chapter these question are answered.

Research question 1. *Can a MR safe pneumatic stepper motor be used to significant reduce the time of a MR guided biopsy?* Primary, biopsy time can be reduced by accurate moving of the needle, such that the position of the needle requires less validation and corrections by the radiologist. De presented actuator has a resolution of 0.5 mm (SD: 0.05 mm). The accuracy of the needle position is predicted to be 0.73 mm, which is a factor 2.7 smaller then the required accuracy of 2 mm.

In addition, the biopsy time can also be reduced by minimalizing the guidance time between two biopts. To be more precise, the time required to switch from one biopt position to another is to be minimalized. The presented actuator achieved a velocity of 70 mm/ sec with 6 m long hoses, which is a factor 3 times larger then other designs.

Research question 2. *How can the velocity of pneumatic actuators be improved, while maintaining the required accuracy?* By using a dual-driven planetary gear, it is possible to increase the velocity, while keeping the ability to create small steps. The presented design uses two pneumatic rotary stepper motors to drive the planetary gear and create the fine and coarse movement of the actuator rod. One of the motors is connented to the carrier of the planetary gear and delivering the coarse movement. A novel actuator, integrated with the ring gear, is developed to drive the ring gear of the planetary gear.

Not only was the actuator able to move a load of 90 N at a pressure of 0.3 MPa. It is completely constructed from MR safe materials too.

The design's drawback is the dimenions and, with the current force requirements, the strength of the housing. Therefore, at the moment, it does not fit in the MR guided manipulator. Despite the drawbacks of the design, the preliminairy results show that the presented actuator is a step in the right direction to reduce the time of a MR guided biopsy.

5.1 Recommendations

The efficiency of the presented actuator could not be derived, because the teeth were broken off of the ring gear and the housing got damaged. Performing a new experiment with proper working actuators is advised to determine the efficiency of the design. Combining the results with the effiencies of each actuator measured seperately, then the efficiency per module can be derived.

The accuracy of each step is measured, however the position accuracy of the actuator is not measured. Repeatability measurements to a certain setpoint can be used to derive the position accuracy of the actuator.

The ring gear of the ring actuator is weak due to the printing process. Printing the parts in two parts and combining them later on avoid the drawback of printing with support. The sun gear, planet gears and carrier can be assembled first and used as aligning tool when the two halves are combined.

The impulses created by the stepping motion of the rotary actuator moves the ring actuator significant. Limiting the movement of the ring actuator by bearings is advisable. Bearings between the housing and outer side of the ring gear is suggested. The ring gear only rotates during fine movement, so these bearings will not produce a lot of heat, so the life time is long.

Another approach is to axial support the ring gear on the output and input shaft, however this makes the manufacturing process more difficult.

Furthermore, the force requirements are expected to be estimated too large. Better research into the forces would give more realistic values and could reduce the dimensions of the design, since less required force results in the use of smaller actuators.

Bibliography

[1] J. Ferlay, I. Soerjomataram, R. Dikshit, S. Eser, C. Mathers, M. Rebelo, D. M. Parkin, D. Forman, and F. Bray, "Cancer incidence and mortality worldwide: Sources, methods and major patterns in GLOBOCAN 2012," *International Journal of Cancer*, vol. 136, no. 5, pp. E359–E386, mar 2015. [Online]. Available: http://doi.wiley.com/10.1002/ijc.29210

[2] M. R. Pokorny, M. de Rooij, E. Duncan, F. H. Schröder, R. Parkinson, J. O. Barentsz, and L. C. Thompson, "Prospective Study of Diagnostic Accuracy Comparing Prostate Cancer Detection by Transrectal UltrasoundâĂŞGuided Biopsy Versus Magnetic Resonance (MR) Imaging with Subsequent MR-guided Biopsy in Men Without Previous Prostate Biopsies," *European Urology*, vol. 66, no. 1, pp. 22–29, jul 2014. [Online]. Available: http://www.ncbi.nlm.nih.gov/pubmed/24666839http://linkinghub.elsevier.com/retrieve/pii/S0302283814002115

[3] P. Zamecnik, M. G. Schouten, A. J. Krafft, F. Maier, H.-P. Schlemmer, J. O. Barentsz, M. Bock, and J. J. Fütterer, "Automated Real-time Needle-Guide Tracking for Fast 3-T MR-guided Transrectal Prostate Biopsy: A Feasibility Study," *Radiology*, vol. 273, no. 3, pp. 879–886, 2014. [Online]. Available: http://dx.doi.org/10.1148/radiol.14132067

[4] D. Stoianovici, A. Patriciu, D. Mazilu, L. Kavoussi, and D. Petrisor, "A New Type of Motor : Pneumatic Step Motor," *IEEE/ASME Transactions on Mechatronics*, vol. 12, no. 1, pp. 98–106, 2007.

[5] V. Groenhuis and S. Stramigioli, "Rapid Prototyping High-Performance Metal Free Pneumatic Stepper Motors," *IEEE/ASME Transactions on Mechatronics*, 2016.

[6] A. Berger, "Magnetic resonance imaging," *BMJâĂŕ: British Medical Journal*, vol. 324(7328), p. 35, 2002. [Online]. Available: https://www.ncbi.nlm.nih.gov/pmc/articles/PMC1121941/pdf/35.pdf

[7] A. G. Van Der Kolk, J. Hendrikse, J. J. M. Zwanenburg, F. Visser, and P. R. Luijten, "Clinical applications of 7 T MRI in the brain," *European Journal of Radiology*, vol. 82, pp. 708–718, 2013.

[8] R. Beisteiner, S. Robinson, M. Wurnig, M. Hilbert, K. Merksa, J. Rath, I. H??llinger, N. Klinger, C. Marosi, S. Trattnig, and A. Gei??ler, "Clinical fMRI: Evidence for a 7T benefit over 3T," *NeuroImage*, vol. 57, no. 3, pp. 1015–1021, 2011.

[9] A. Peltier, F. Aoun, M. Lemort, F. Kwizera, M. Paesmans, and R. Van Velthoven, "MRI-targeted biopsies versus systematic transrectal ultrasound guided biopsies for the diagnosis of localized prostate cancer in biopsy na??ve men," *BioMed Research International*, vol. 2015, p. 6, 2015.

[10] M. G. Schouten, C. M. Hoeks, J. G. Bomers, C. A. Hulsbergen-van de Kaa, J. A. Witjes, L. C. Thompson, M. M. Rovers, J. O. Barentsz, and J. J. Futterer, "Location of Prostate Cancers Determined by Multiparametric and MRI-Guided Biopsy in Patients With Elevated Prostate-Specific Antigen Level and at Least One Negative Transrectal Ultrasound-Guided Biopsy," *Ajr*, vol. 205, no. 1, pp. 57–63, 2015.

[11] M. Rashid and F. Kibria. Accessed: 19-01-2017. [Online]. Available: http://snc2dmri.weebly.com/components--functions.html

[12] F. G. Shellock, "Chapter 16 MRI Issues for Implants and Devices," in *MRI Bioeffects, Safety, and Patient Management*, F. G. Shellock and J. V. Crues, Eds., 2014, pp. 375–394.

[13] ASTM F2503-05, "Standard Practice for Marking Medical Devices and Other Items for Safety in the Magnetic Resonance Environment 1," West Conshohocken, PA, 2005. [Online]. Available: www.astm.org

[14] A. Krieger, N. B. Cho, I. Iordachita, P. Guion, G. Fichtinger, and L. L. Whitcomb, "Development and Evaluation of an Actuated MRI-Compatible Robotic System for MRI-Guided Prostate Intervention," *IEEE/ASME Transactions on Mechatronics*, vol. 18, no. 1, pp. 273–284, 2013.

[15] P. Moreira and S. Misra, "MR-Compatible Robot for Needle-Based Prostate Interventions," University of Twente; University of Groningen and University of Medical Center Groningen, Tech. Rep., 2016.

[16] T. Mashimo, S. Toyama, and H. Matsuda, "Development of rotary-linear piezoelectric actuator for MRI compatible manipulator," in *2008 IEEE/RSJ International Conference on Intelligent Robots and Systems*. IEEE, sep 2008, pp. 113–118. [Online]. Available: http://ieeexplore.ieee.org/document/4650623/

[17] T. Mashimo and S. Toyama, "MRI-Compatibility of a Manipulator using a Spherical Ultrasonic Motor," in *The 12th World Congress in Mechanism and Machine Science (IFToMM2007)*, 2007.

[18] G. S. Fischer, A. Krieger, I. Iordachita, C. Csoma, L. L. Whitcomb, and G. Fichtinger, "MRI Compatibility of Robot Actuation Techniques – A Comparative Study," in *Medical Image Computing and Computer-Assisted Intervention – MICCAI 2008: 11th International Conference, New York, NY, USA, September 6-10, 2008, Proceedings, Part II*, D. Metaxas, L. Axel, G. Fichtinger, and G. Székely, Eds. Springer Berlin Heidelberg, 2008, pp. 509–517. [Online]. Available: http://dx.doi.org/10.1007/978-3-540-85990-1{_}61

[19] D. Stoianovici, D. Song, D. Petrisor, D. Ursu, D. Mazilu, M. Muntener, M. Mutener, M. Schar, and A. Patriciu, "MRI Stealth robot for prostate interventions." *Minimally invasive therapy & allied technologies : MITAT : official journal of the Society for Minimally Invasive Therapy*, vol. 16, no. 4, pp. 241–8, 2007. [Online]. Available: http://www.ncbi.nlm.nih.gov/pubmed/17763098

[20] D. Chapuis, R. Gassert, G. Ganesh, E. Burdet, and H. Bleuler, "Investigation of a Cable Transmission for the Actuation of MR Compatible Haptic Interfaces," in *The First IEEE/RAS-EMBS International Conference on Biomedical Robotics and Biomechatronics, 2006. BioRob 2006*. IEEE, 2006, pp. 426–431. [Online]. Available: http://ieeexplore.ieee.org/document/1639125/

[21] G. Ganesh, R. Gassert, E. Burdet, and H. Bleuler, "Dynamics and control of an MRI compatible master-slave system with hydrostatic transmission," in *IEEE International Conference on Robotics and Automation, 2004. Proceedings. ICRA '04. 2004*. IEEE, 2004, pp. 1288–1294 Vol.2. [Online]. Available: http://ieeexplore.ieee.org/document/1308002/

[22] N. Yu, C. Hollnagel, A. Blickenstorfer, S. Kollias, and R. Riener, "fMRI-Compatible Robotic Interfaces with Fluidic Actuation," *Robotics: Science and Systems*, pp. 199–205, 2009.

[23] S. Zangos, A. Melzer, K. Eichler, C. Sadighi, A. Thalhammer, B. Bodelle, R. Wolf, T. Gruber-Rouh, D. Proschek, R. Hammerstingl, C. Müller, M. G. Mack, and T. J. Vogl, "MR-compatible Assistance System for Biopsy in a High-Field-Strength System: Initial Results in Patients with Suspicious Prostate Lesions," *Radiology*, vol. 259, no. 3, pp. 903–910, 2011. [Online]. Available: http://dx.doi.org/10.1148/radiol.11101559

[24] J. G. R. Bomers, D. G. H. Bosboom, G. H. Tigelaar, J. Sabisch, J. J. Fütterer, and D. Yakar, "Feasibility of a 2nd generation MR-compatible manipulator for transrectal prostate biopsy guidance," *European Radiology*, pp. 1—-7, 2016. [Online]. Available: http://dx.doi.org/10.1007/s00330-016-4504-2

[25] T. A. Stamey, F. S. Freiha, J. E. McNeal, E. A. Redwine, A. S. Whittemore, and H.-P. Schmid, "Localized prostate cancer. Relationship of tumor volume to clinical significance for treatment of prostate cancer," *Cancer*, vol. 71, no. S3, pp. 933–938, feb 1993. [Online]. Available: http://doi.wiley.com/10.1002/

1097-0142{%}2819930201{%}2971{%}3A3{%}2B{%}3C933{%}3A{%}3AAID-CNCR2820711408{%}3E3.0.CO{%}3B2-L

[26] DEMCON, "MIRIAM System Requirements Document 2014-04-02," Tech. Rep., 04 2014.

[27] R. A. Beier, "Pressure Response of a Pneumatic System," *the Technology Interface Journal/Spring*, vol. 9, no. 2, pp. 1523–9926, 2009. [Online]. Available: http://technologyinterface.nmsu.edu/Spring09/

[28] N. H. Beachley and A. A. Frank, "Continuously variable transmissions: theory and practice," Ph.D. dissertation, University of Wisconsin, Madison, 1979. [Online]. Available: https://www.osti.gov/scitech/servlets/purl/5529813/

[29] N. Srivastava and I. Haque, "A review on belt and chain continuously variable transmissions (CVT): Dynamics and control," *Mechanism and Machine Theory*, vol. 44, no. 1, pp. 19–41, 2009. [Online]. Available: http://www.sciencedirect.com/science/article/pii/S0094114X08001432

[30] P. Spanoudakis and N. C. Tsourveloudis, "On the efficiency of a prototype continuous variable transmission system," in *21st Mediterranean Conference on Control and Automation*. IEEE, jun 2013, pp. 290–295. [Online]. Available: http://ieeexplore.ieee.org/document/6608736/

[31] Jinming Liu and Huei Peng, "Modeling and Control of a Power-Split Hybrid Vehicle," *IEEE Transactions on Control Systems Technology*, vol. 16, no. 6, pp. 1242–1251, nov 2008. [Online]. Available: http://ieeexplore.ieee.org/document/4475524/

[32] E. Gouda, S. Mezani, L. Baghli, and A. Rezzoug, "Comparative Study Between Mechanical and Magnetic Planetary Gears," *IEEE Transactions on Magnetics*, vol. 47, no. 2, pp. 439–450, feb 2011. [Online]. Available: http://ieeexplore.ieee.org/document/5620982/

[33] Y. C. Wu and C. W. Chang, "Development of 3-speed rear hub bicycle transmissions with gear-shifting mechanisms," *Transactions of the Canadian Society for Mechanical Engineering*, 2015.

[34] K. Seki, Y. Shinohara, M. Iwasaki, H. Chinda, and M. Takahashi, "Force controller design based on PQ method for dual-stage actuators in polishing machines," in *IECON 2011 - 37th Annual Conference of the IEEE Industrial Electronics Society*. IEEE, nov 2011, pp. 3388–3393. [Online]. Available: http://ieeexplore.ieee.org/document/6119856/

[35] J. B. Morrell and J. K. Salisbury, "In pursuit of dynamic range: Using parallel coupled actuators to overcome hardware limitations," in *Experimental Robotics IV*. London: Springer-Verlag, 1997, pp. 263–273. [Online]. Available: http://www.springerlink.com/index/10.1007/BFb0035217

[36] Hoyul Lee, Chulwoo Lee, Seongjin Kim, and Youngjin Choi, "New actuator system using movable pulley for bio-mimetic system and wearable robot applications," in *2010 IEEE International Conference on Robotics and Automation*. IEEE, may 2010, pp. 2183–2188. [Online]. Available: http://ieeexplore.ieee.org/document/5509989/

[37] H. Lee and Y. Choi, "A New Actuator System Using Dual-Motors and a Planetary Gear," *IEEE/ASME Transactions on Mechatronics*, vol. 17, no. 1, pp. 192–197, feb 2012. [Online]. Available: http://ieeexplore.ieee.org/document/6022796/

[38] M. P. Van Gellekom, M. A. Moerland, J. J. Battermann, and J. J. Lagendijk, "MRI-guided prostate brachytherapy with single needle methodâĂŤa planning study," *Radiotherapy and Oncology*, vol. 71, no. 3, pp. 327–332, 2004.

[39] B.-R. Höhn, K. Stahl, and P. Gwinner, "Light-Weight Design for Planetary Gear Transmissions," *GEAR TECHNOLOGY*, pp. 96–103, 2013. [Online]. Available: http://www.geartechnology.com/issues/0913x/light-weight-planetary.pdf

[40] E. Edge, "Lewis Factor Equation for Gear Tooth Calculations - Engineers Edge." [Online]. Available: http://www.engineersedge.com/gears/lewis-factor.htm

[41] W. Dornfeld, "Stresses on Spur Gear Teeth," 2006. [Online]. Available: http://www.faculty.fairfield.edu/wdornfeld/ME312/ToothLoads04.pdf

[42] Grooved ball bearing xirodur b180. Accessed: 30-08-2017. [Online]. Available: http://www.igus.eu/wpck/15421/xirodur_B180_kaefige

[43] Arduino ide. Accessed: 30-08-2017. [Online]. Available: https://www.arduino.cc

[44] A. Elster. (2017) Questions and answers in mri. Accessed: 22-08-2017. [Online]. Available: http://www.mriquestions.com

A Drawing and dimensions of the design

In total five drawings are generated of the design: 1) Planetary gear; 2) Ring gear; 3) Rack-pinion mechanism; 4) Ring actuator; 5) Rotary actuator; and 6) Housing.

2D rev._ver.	Revision description	Revised by / date
		/

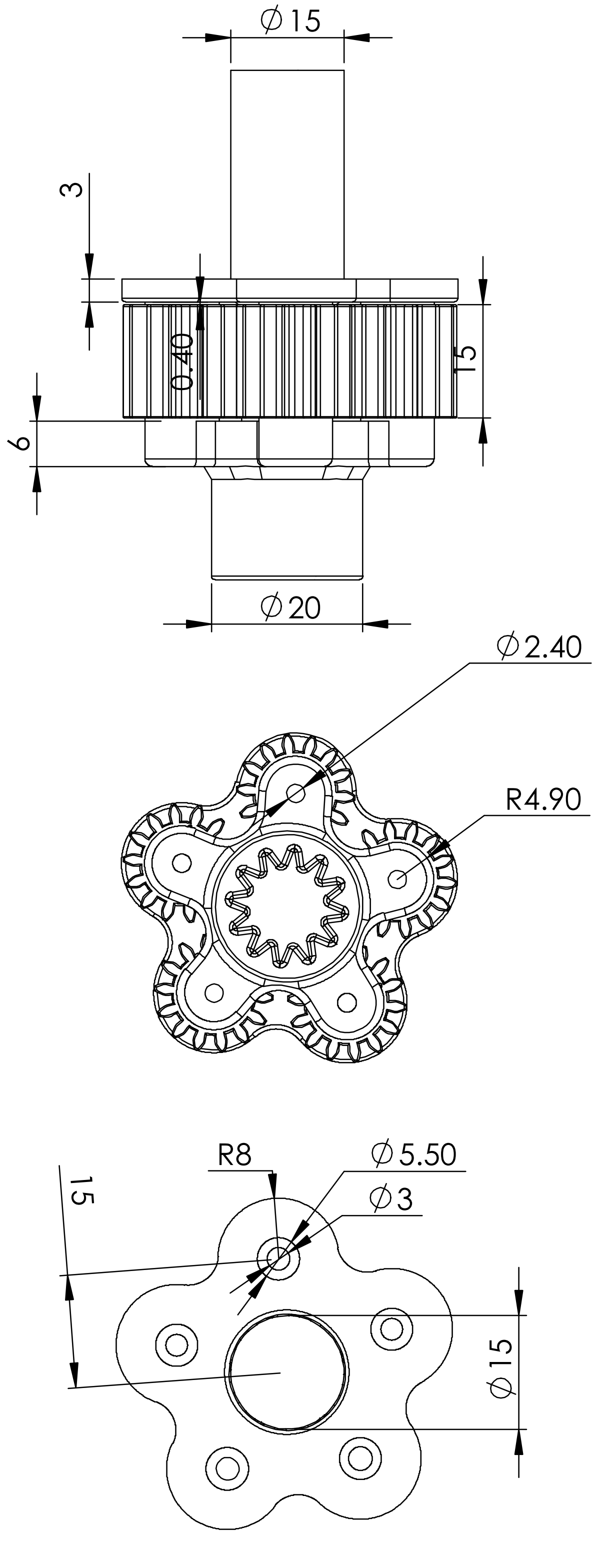

Am. proj.	Scale:	Units:	Sheet:	Form:	Drawn by / date:	by:
	1:1	mm	1 of 1	A4	/	/

DEMCON
advanced mechatronics

Description:		
From 3D: planetary_v1_assem	3D rev._ver.:	Comp. type:
Drawing nr.: planetary_v1_assem		2D rev._ver.:

tel. +31 (0)88 115 20 00

2D rev._ver.	Revision description	Revised by / date
		/

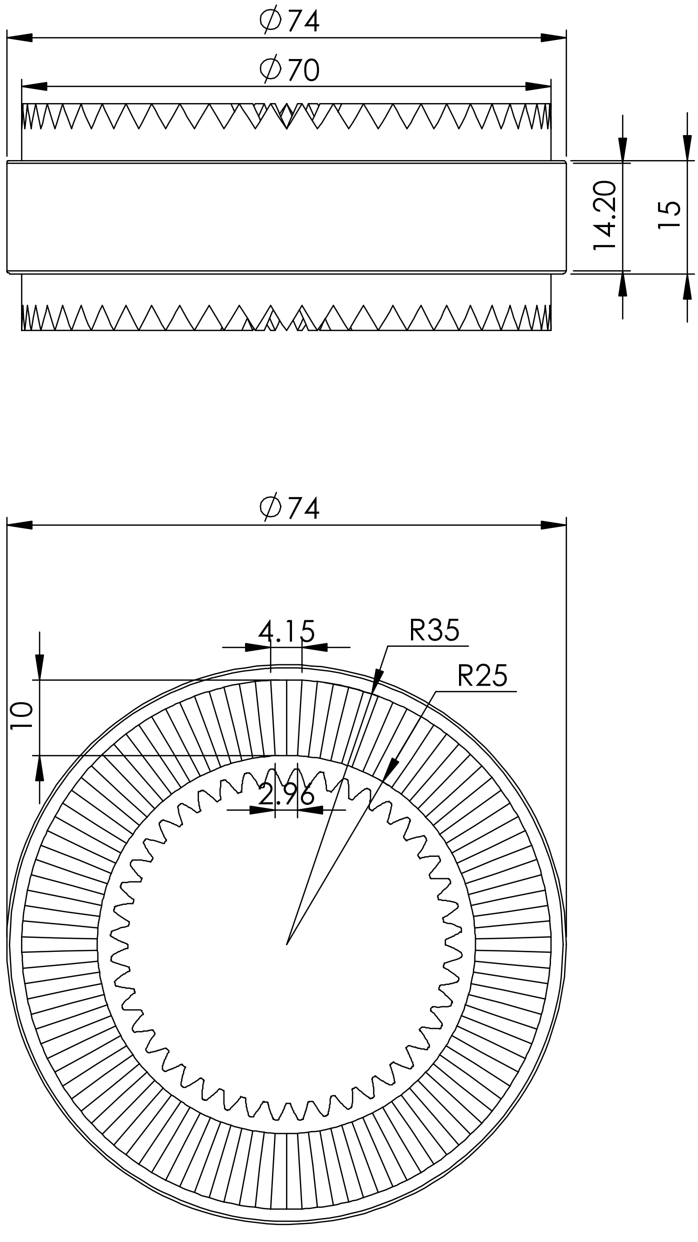

Am. proj.	Scale:	Units:	Sheet:	Form:	Drawn by / date:	by:
	1:1	mm	1 of 1	A4	/	/

DEMCON
advanced mechatronics

Description:

From 3D: ring_assembly
3D rev._ver.:
Comp. type:

Drawing nr.:
ring_assembly
2D rev._ver.:

tel. +31 (0)88 115 20 00

2D rev._ver.	Revision description	Revised by / date
		/

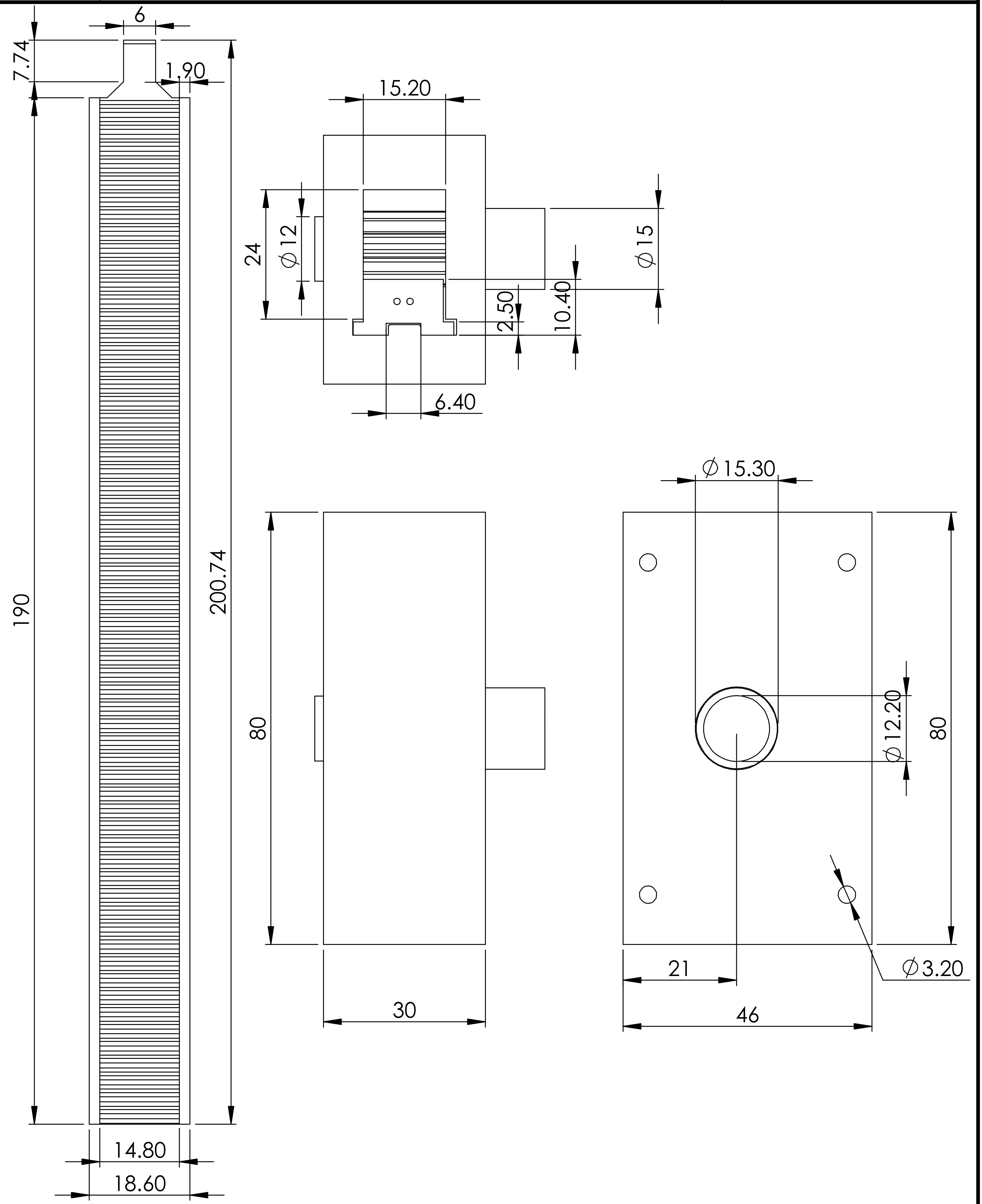

Am. proj.	Scale:	Units:	Sheet:	Form:	Drawn by / date:	by:
	1:1	mm	1 of 1	A4	/	/

DEMCON
advanced mechatronics

tel. +31 (0)88 115 20 00

Description:

From 3D: rack-pinion 3D rev._ver.: Comp. type:

Drawing nr.: rack-pinion 2D rev._ver.:

2D rev._ver.	Revision description	Revised by / date
		/

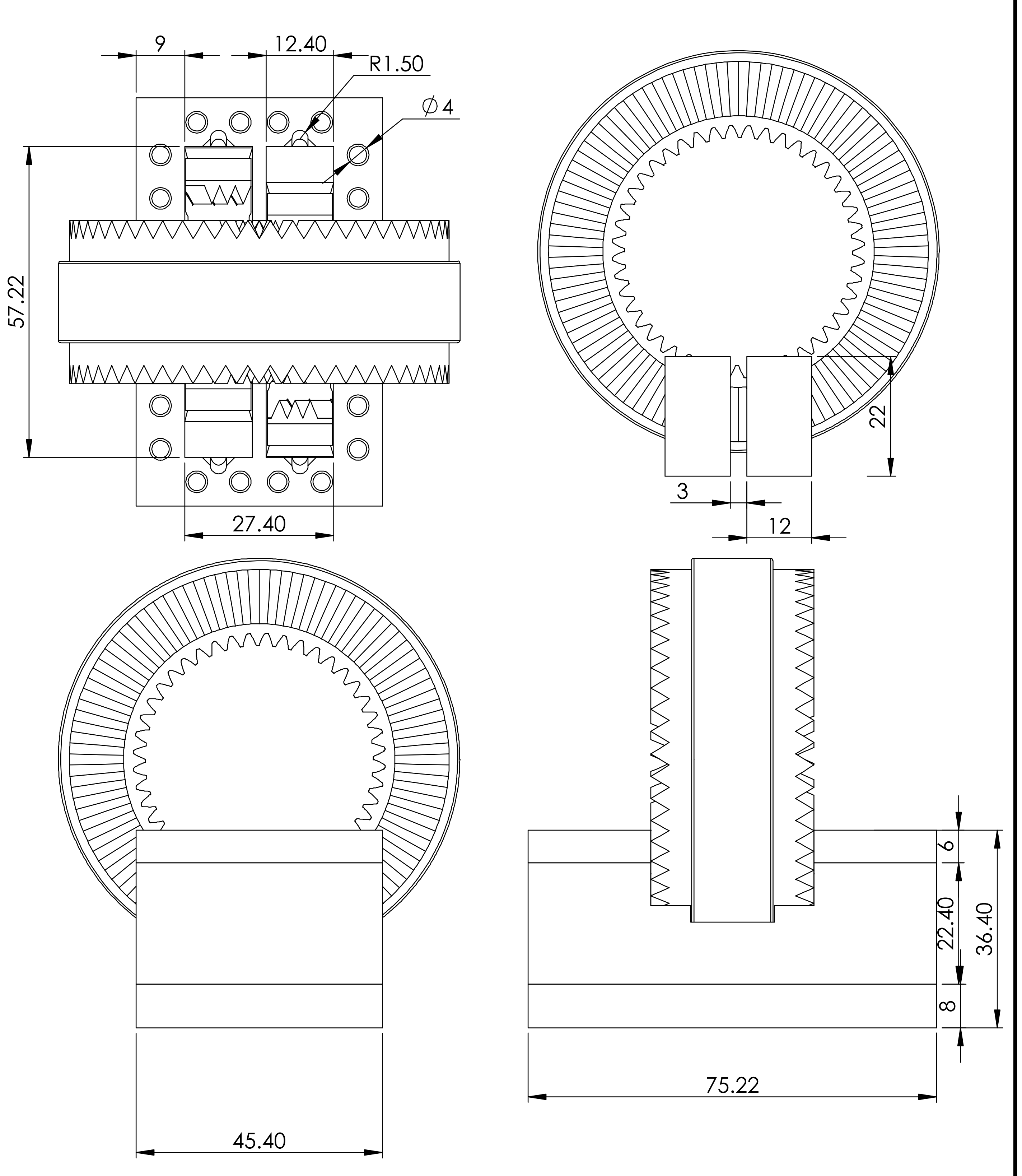

Am. proj.	Scale: 1:1	Units: mm	Sheet: 1 of 1	Form: A4	Drawn by / date: /	by: /

DEMCON

advanced mechatronics

tel. +31 (0)88 115 20 00

Description:

From 3D: Assem_3mm_total_act_v1 3D rev._ver.: Comp. type:

Drawing nr.: Assem_3mm_total_act_v1 2D rev._ver.:

2D rev._ver.	Revision description	Revised by / date
		/

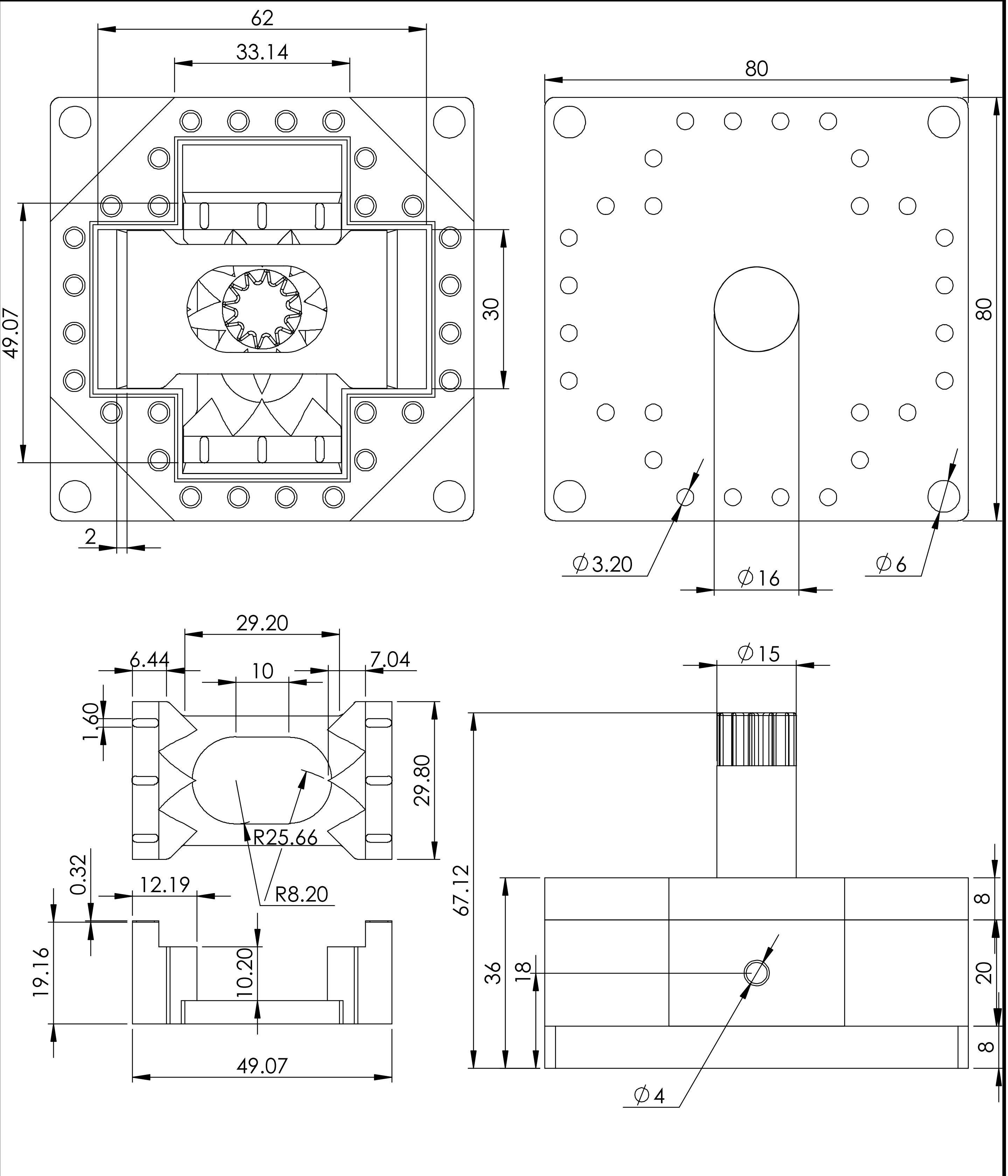

Am. proj.	Scale: 1:1	Units: mm	Sheet: 1 of 1	Form: A4	Drawn by / date: /	by: /

DEMCON
advanced mechatronics

tel. +31 (0)88 115 20 00

Description:

From 3D: M_R-80_Assembly | 3D rev._ver.: | Comp. type:

Drawing nr.: M_R-80_Assembly | 2D rev._ver.:

2D rev._ver.	Revision description	Revised by / date
		/

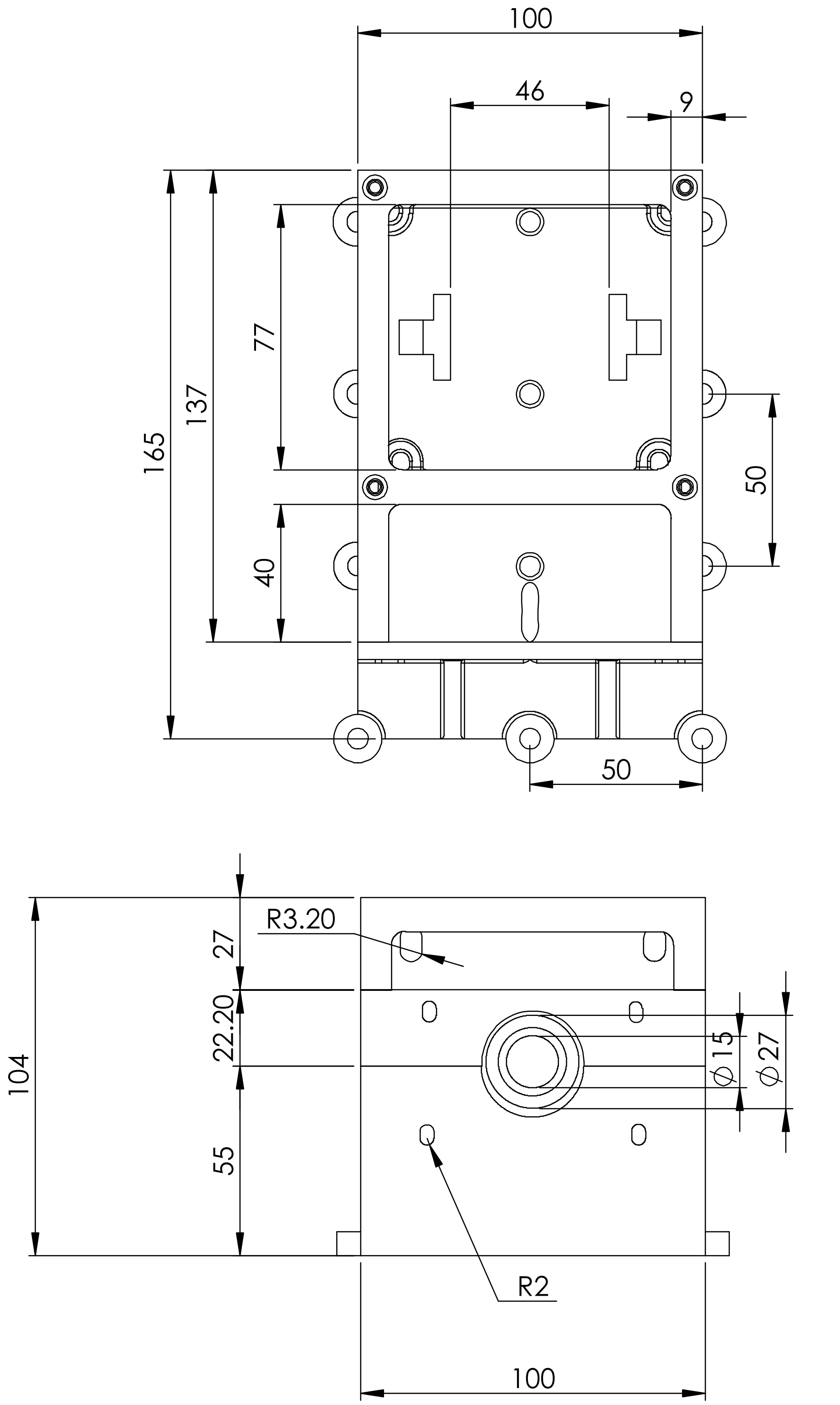

Am. proj.	Scale:	Units:	Sheet:	Form:	Drawn by / date:	by:
	1:2	mm	1 of 1	A4	/	/

DEMCON
advanced mechatronics

Description:

From 3D: housing_all_parts 3D rev._ver.: Comp. type:

Drawing nr.: housing_all_parts 2D rev._ver.:

tel. +31 (0)88 115 20 00